Received: 10 September 2018 | Revised: 28 November 2018 | Accepted: 30 November 2018
DOI: 10.1002/glia.23580

GLIA
WILEY

RESEARCH ARTICLE

Melanopsin for precise optogenetic activation of astrocyte-neuron networks

Sara Mederos[1] | Alicia Hernández-Vivanco[1] | Jorge Ramírez-Franco[1] | Mario Martín-Fernández[2] | Marta Navarrete[3] | Aimei Yang[4] | Edward S. Boyden[4,5] | Gertrudis Perea[1]

[1]Department of Functional and Systems Neurobiology, Instituto Cajal, CSIC, Madrid, Spain

[2]Department of Neuroscience, University of Minnesota, Minneapolis, Minnesota

[3]Centro de Biología Molecular Severo Ochoa (CSIC-UAM), Madrid, Spain

[4]Media Lab, Massachusetts Institute of Technology, Cambridge, Massachusetts

[5]McGovern Institute, Massachusetts Institute of Technology, Cambridge, Massachusetts

Correspondence
Dr. Gertrudis Perea, Instituto Cajal, CSIC, Avda. Doctor Arce, 37, Madrid 28002, Spain.
Email: gperea@cajal.csic.es

Funding information
Ministerio de Economía y Competitividad, Grant/Award Number: BES-2014-067594BFU2013-47265RBFU2016-75107-PIntramural 201620I017

Abstract

Optogenetics has been widely expanded to enhance or suppress neuronal activity and it has been recently applied to glial cells. Here, we have used a new approach based on selective expression of melanopsin, a G-protein-coupled photopigment, in astrocytes to trigger Ca^{2+} signaling. Using the genetically encoded Ca^{2+} indicator GCaMP6f and two-photon imaging, we show that melanopsin is both competent to stimulate robust IP3-dependent Ca^{2+} signals in astrocyte fine processes, and to evoke an ATP/Adenosine-dependent transient boost of hippocampal excitatory synaptic transmission. Additionally, under low-frequency light stimulation conditions, melanopsin-transfected astrocytes can trigger long-term synaptic changes. In vivo, melanopsin-astrocyte activation enhances episodic-like memory, suggesting melanopsin as an optical tool that could recapitulate the wide range of regulatory actions of astrocytes on neuronal networks in behaving animals. These results describe a novel approach using melanopsin as a precise trigger for astrocytes that mimics their endogenous G-protein signaling pathways, and present melanopsin as a valuable optical tool for neuron–glia studies.

Main points: Melanopsin, a mammalian G-protein-coupled photopigment, engages endogenous the IP3 pathway and intracellular Ca^{2+} signaling in astrocytes.

By releasing ATP/Ado, melanopsin-astrocytes differently impact synaptic plasticity enhance cognitive functions.

KEYWORDS

astrocytes, optogenetics, melanopsin, neuron–glia interactions, synaptic plasticity

1 | INTRODUCTION

The outbreak practice of optical tools to enhance or suppress neuronal activity and to decipher the organization of brain circuits and their behavioral outputs has transformed Neuroscience (Bernstein & Boyden, 2011). Some recent studies have applied these approaches to glial cells, particularly to astrocytes, to unmask the consequences of astrocyte signaling on particular brain functions. Photostimulation with channelrhodopsin-2 (ChR2; Gourine et al., 2010; Masamoto et al., 2015; Pelluru, Konadhode, Bhat, & Shiromani, 2016; Perea, Yang, Boyden, & Sur, 2014; Sasaki et al., 2012; Yamashita et al., 2014), a nonspecific cation channel, and Archaerhodopsin (Arch; Letellier et al., 2016; Poskanzer & Yuste, 2016), a light-driven proton pump, have being frequently used to manipulate intracellular Ca^{2+} signals in astrocytes and determine their role in specific brain functions. However, whether the intracellular astrocyte Ca^{2+} signaling triggered by these opsins recapitulates physiologically Ca^{2+} signaling, which is mostly mediated by G-protein coupled receptor (GPCR) activation, is under debate (Xie, Petravicz, & McCarthy, 2015). Alternatively, the engineered G-protein coupled receptors activated by inert drug-like small molecules (DREADDs) have been also applied for astrocyte-neuron studies revealing the impact of astrocyte signaling in food intake (Chen et al., 2016; Yang, Qi, & Yang, 2015), fear responses (Martin-Fernandez et al., 2017), memory recall (Adamsky et al., 2018),

Sara Mederos and Alicia Hernández-Vivanco contributed equally to this work.

and autonomic nervous system responses (Agulhon et al., 2013) (for a review see [Bang, Kim, & Lee, 2016]). However, those effects rely on a sustained activation of DREADDs by its exogenous ligand, misplacing the temporal features of astrocyte signaling engaged by neuronal activity. Therefore, refined and reliable approaches involving endogenous astrocyte Ca^{2+} signaling in a time-controlled manner are still required.

In order to expand the available tools allowing a fast control of astrocyte signaling, we focused on melanopsin, a G-protein-coupled photopigment expressed by a small subset of mammalian retinal ganglion cells, with an absorption peak around 470–480 nm (Hatori & Panda, 2010; Hattar, Liao, Takao, Berson, & Yau, 2002; Sexton, Buhr, & Van Gelder, 2012). In contrast to the algae-derived opsins[20], melanopsin couples to $G\alpha_{q\text{-}11}$ to activate PLCβ, leading to the IP3 signaling and the elevation of intracellular Ca^{2+} levels (Panda et al., 2005). The similarities of melanopsin with other $G\alpha_{q\text{-}11}$-coupled GPCRs for neurotransmitters, including α1-adrenergic, cholinergic M1 and mGluR group 1 receptors, make it an appropriate optical tool for astrocytes. We designed a new construct fusing *gfap* promoter with melanopsin (*Opn4*-human melanospin) using viral strategy to target astrocytes and evaluate whether melanopsin was competent to both stimulate Ca^{2+} activity in astrocytes, measured by the expression of genetically encoded Ca^{2+} indicators (GCaMP6f), and to induce astrocyte-to-neuron signaling. Our results reveal that blue light-evoked substantial Ca^{2+} responses at small regions of astrocyte processes and short-term EPSCs changes in CA1 hippocampal neurons. We found that melanopsin engaged endogenous G-protein and IP3 signaling pathways in astrocytes and could stimulate the release of ATP/Adenosine, which mediated the synaptic enhancement; and glutamate, responsible of the NMDA-dependent slow inward currents in CA1 neurons. In contrast to melanopsin, astrocyte Ca^{2+} signals induced by ChR2 stimulation were noticed after longer light pulses, which resulted in sustained synaptic modifications. Low-frequency stimulation of melanopsin-expressing astrocytes triggered long-term synaptic plasticity (LTP). Finally, to evaluate the impact of astrocyte signaling in cognitive performance, in vivo activation of melanopsin-astrocytes was performed. Our data indicated that melanopsin-transfected mice showed an enhanced ability to discriminate object location, suggesting an improved memory performance. These data show that astrocytes could modulate their functional impact on neuronal networks depending on different patterns of synaptic activity, which can be mimicked by melanopsin stimulation. Overall, this study describes melanopsin as previously unidentified tool for optical activation of astrocytes, which is revealed as a meaningful G-protein signaling mechanism and a valuable approach for in vivo neuron–glia studies.

2 | MATERIALS AND METHODS

2.1 | Mice

All the procedures for handling and sacrificing animals followed the European Commission guidelines for the welfare of experimental animals (2010/63/EU). Animals of both genders were used, and were housed in standard laboratory cages with ad libitum access to food and water, under a 12:12 hr dark–light cycle in temperature-controlled rooms. C57BL/6 wild-type mice and *Ip3r2*$^{-/-}$ (RRID: MGI:3640970) mice were used. *Ip3r2*$^{-/-}$ mice were generously donated by Dr. J. Chen (University of California San Diego, CA; X. Li, Zima, Sheikh, Blatter, & Chen, 2005).

2.2 | Viral injection

The following constructs were used: ChR2 (AAV2/5-GFAP104-ChR2-mCherry; UNC Vector Core; viral titer 3.9×10^{12}), GCaMP6f (AAV2/5-Gfap-Lck-GCaMP6f; PENN Vector Core; viral titer 6.4×10^{13}), vector (AAV2/5-Gfap-mCherry; UNC Vector Core; viral titer 3.9×10^{12}). Melanopsin (*Opn4*-human melanopsin, AAI13559.1) was fused to mCherry and cloned into AAV particles (serotype 5; UNC Vector Core) using the GFAP promoter short version GFAP104 (AAV2/5-GFAP104-melanopsin-mCherry; viral titer 2.8×10^{12}). Neonatal wild-type and *Ip3r2*$^{-/-}$ mice (P5-8) were anesthetized with isoflurane 2% in oxygen and place in a custom adapted stereotaxic apparatus. The target coordinates were displaced from Bregma by 2 mm posterior, 1.4 mm lateral and 1.2–1.4 mm dorsoventral. A volume of 0.3 μL of the virus at 30 nL/min was injected. After injection, the pipette was held in place for 5 min prior to retraction to prevent leakage and then removed and skin sutured. The animal was allowed to recover from anesthesia with the help of heating pads and was returned to the cage once it showed regular breathing and locomotion. The overall duration of this procedure was kept under 20 min so as to maximize the survival rate of the pups. For a subset of experiments cytoGCaMP6f (AAV2/5-Gfap-cyto-GCaMP6f; PENN Vector Core; viral titer 6.13×10^{13}) was transfected in hippocampal astrocytes. After 2 weeks of viral injection, specific astrocytes expression of constructs was confirmed by immunostaining (Figure 1b and Supporting Information Figures S1 and S2). In core regions of transfection, GFAP staining and mCherry expression colocalized in astrocytes, while no colocalization was observed in NeuN labeled neurons. For Ca^{2+} imaging experiments, lck-GCaMP6f or cytoGCaMP6f was co-injected with melanopsin, ChR2 or vector (1:1 ratio).

2.3 | Hippocampal slice preparation

Imaging and electrophysiological experiments were performed on hippocampal slices from P20–P30 mice. The brain was rapidly removed and placed in ice-cold artificial cerebrospinal fluid (ACSF). Slices (350 μm) obtained with a vibratome (Leica Vibratome VT1200S, Germany) were incubated during >1 hr at room temperature (22–24°C) in ACSF containing [in mM]: NaCl 124, KCl 2.69, KH_2PO_4 1.25, $MgSO_4$ 2, $NaHCO_3$ 26, $CaCl_2$ 2, and glucose 10, and was gassed with 95% O_2/5% CO_2 (pH = 7.3). Slices were then transferred to an immersion recording chamber and perfused with gassed ACSF. Cells were visualized with an Olympus BX50WI or Nikon Eclipse FN1 microscope coupled with a 40× water immersion lens and infrared-DIC optics.

2.4 | Electrophysiology

Two weeks after viral injection, electrophysiological recordings from CA1 pyramidal neurons and astrocytes were made using the whole-cell configuration of the patch-clamp technique. Patch electrodes had

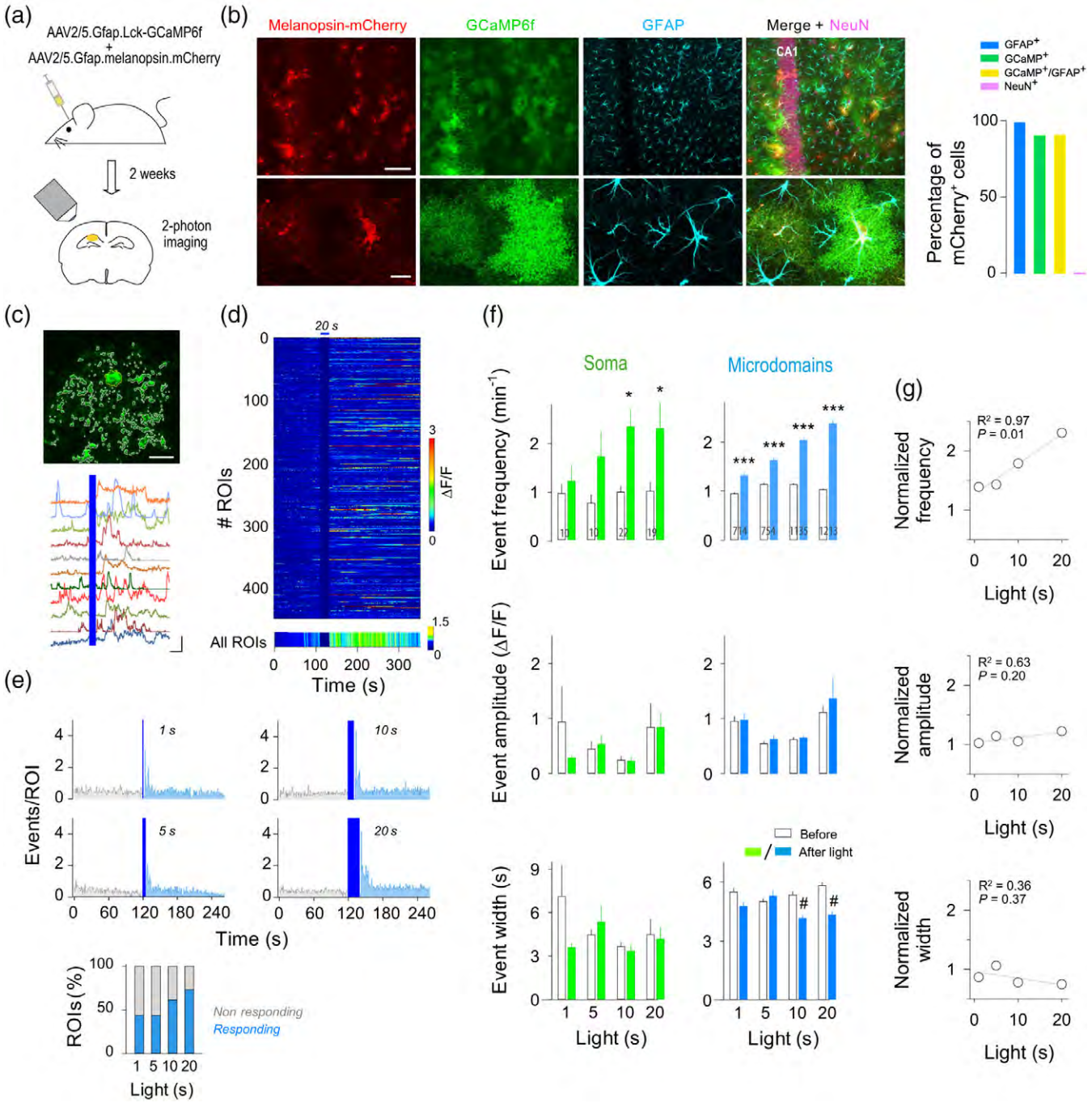

FIGURE 1 Selective expression of melanopsin in astrocytes stimulates Ca^{2+} signaling. (a) Scheme of the experimental approach. *Top*, viral transfection of AAV2/5-Gfap-Lck.GCaMP6f and AAV2/5-Gfap-melanopsin-mCherry in hippocampus. *Bottom:* hippocampal slice under two-photon imaging after 2 weeks of transfection. (b) *Top*: Immunocytochemical localization of melanopsin-mCherry, GCaMP6f, and GFAP in hippocampal slices; *bottom*: a detailed image of labeled astrocytes. *Merge* includes NeuN labeling (pink). Scale bar, 50 μm; inset, 10 μm. *Right*: percentage of GFAP (98.72 ± 0.88%), GCaMP6f (90.42 ± 3.23%) and NeuN-positive cells (0%) out of mCherry positive cells (n = 138; 12 fields of view; two mice), showing the selective expression of mCherry reporter for melanopsin in astrocytes. (c) *Top*: image of GCaMP6f-melanopsin astrocyte (top) and selected microdomains identified by GECIquant on ImageJ mask generator (bottom). *Bottom*: representative intensity Ca^{2+} signals versus time evoked by melanopsin light stimulation (20 s; blue bar). Scale bar = 15 μm; 3 ΔF/F, 50 s. (d) Representative raster plot of ROIs activity, color coded according to fluorescence change (top, n = 450), and average microdomain population activity versus time before and after 20 s light (bottom, n = 1,213). (e) *Top*: histogram of ROIs event frequency versus time for each condition (1 s, n = 714; 5 s, n = 757; 10 s, n = 1,135; 20 s, n = 1,213; 41 slices from nine mice). *Bottom*, percentage of ROIs showing an event during the first 20 s after light stimulation (Responding ROI) (1 s n = 313; 5 s n = 331; 10 s n = 697; 20 s n = 891). (f) *Left*: analysis of somatic Ca^{2+} fluctuation properties, measured in Lck-GCaMP6f, showing mean responses for event frequency, amplitude and width (1 s: n = 10; 5 s: n = 10; 10 s: n = 22; 20 s: n = 19; 41 slices from nine mice). Resting versus light 10 s, p = 0.034; 20 s, p = 0.043; two-way ANOVA analysis, post hoc comparison with Tukey–Kramer test. *Right*: analysis of microdomain Ca^{2+} event properties (1 s, n = 714 out of 877 (81.42%); 5 s, n = 757 out 939 (80.62%); 10 s, n = 1,135 out of 1,326 (85.60%); 20 s, n = 1,213 out of 1,333 (90.99%); 41 slices from nine mice). *p < 0.05, ** p < 0.01, ***, # p < 0.001; two-way ANOVA, post hoc comparison with Tukey–Kramer test. (g) Normalized changes in frequency, amplitude and width of microdomain events to resting conditions. Linear fitting between different stimuli conditions, R^2 is shown for each graph. Data are shown as mean ± *SEM*

resistances of 3–5 MΩ when filled with the internal solution that contained for neurons (in mM): KGluconate 135, KCl 10, HEPES 10, $MgCl_2$ 1, ATP-Na_2 2, titrated with KOH to pH 7.3; and for astrocytes (in mM): potassium methanesulfonate 100, KCl 50, HEPES-K 10, ATP-Na_2 2 (pH = 7.3 adjusted with KOH; osmolality 280–290 mOsm/L). Recordings were obtained with PC-ONE amplifier (Dagan Corporation, Minneapolis, MN). Series and input resistances were monitored throughout the experiment using a −5 mV pulse. Mean input resistance was 3.90 ± 0.26 MΩ and mean amplitude of background noise was 0.27 ± 0.09 pA (peak to peak mean amplitude of 4.47 ± 0.79 pA from a representative sample of 15 recorded cells). Recordings were rejected when the access resistance increased >20% during the experiment. Signals were fed to a Pentium-based PC through a DigiData 1,440 interface board (Molecular Devices, San Jose, CA). The pCLAMP 10.2 software (Molecular Devices) was used for data display, acquisition, and storage. Experiments were performed at room temperature (21–24°C). Cells were voltage-clamped at −70 mV. ACSF included picrotoxin (50 μM) and CGP 55845 (5 μM) for EPSC recordings, and TTX (1 μM) for mEPSCs. Synaptic stimulation was achieved using theta capillaries (2–5 μm tip diameter) filled with ACSF, and placed in the *stratum radiatum* to stimulate Schaffer collateral fibers. Paired pulses (250 μs duration; 75 ms interval) were delivered at 0.33 Hz by stimulator S-900 (Dagan Corporation). Baseline of synaptic activity was measured 3–5 min before astrocyte stimulation. Neurons showing *z*-score > 2 standard deviation (*SD*) of baseline EPSC amplitude (pA) during the first 5 min after stimulation were considered responding to light (Figures 2a, 3e, 5c, and 7d). To estimate the EPSC variance modifications after light stimuli, neurons that showed *z*-score > 2 were selected for the analysis of the noise-free coefficient of variation (CV_{NF}) of synaptic responses for the case of melanopsin or ChR2 transfected slices (1, 10, and 30 min after stimulus, as indicated in the figures). $CV_{NF} = \sqrt{(SD\ EPSC^2 - SD\ noise^2)}/m$; SD $EPSC^2$ and SD $noise^2$ are the variance of the peak EPSC and baseline, respectively, and *m* is the mean EPSC peak amplitude. The ratio of CV was obtained for each neuron in control and light conditions as CV_{NF} after light/CV_{NF} control (Fernandez de Sevilla, Cabezas, de Prada, Sanchez-Jimenez, & Buno, 2002). Plots comparing variation in Normalized EPSC amplitude (mean peak amplitude after light stimulus/mean peak amplitude in control conditions) against (CV^{-2}) in each cell were represented. CV_{NF} is commonly used to detect changes in presynaptic transmitter release (Faber & Korn, 1991). For the case of vector-transfected astrocytes, nontransfected astrocytes and *Ip3r2*$^{-/-}$ mice CV_{NF} was analyzed for all the recorded neurons. Changes in the holding current after light stimulation were monitored by analyzing the Holding current index: [holding current (*i*) - holding current (baseline)]/ absolute value [holding current (*i*) + holding current (baseline)]. *i* = holding current values at different time after light stimulus. Experiments designed to optimize NMDAR activation and recording slow inward currents (SIC) were done in a modified Mg^{2+}-free ACSF (Mg^{2+} was equimolarly substituted by Ca^{2+}) plus TTX (1 μM). Drugs were bath applied (for indicated experiments drugs were applied for at least 15 min before recordings). Slow inward currents both spontaneous and opsin-induced were discriminated from standard miniature EPSCs (mEPSCs) based on their time courses, that is, rise and decay time (Figure 6c; cf. [Perea & Araque, 2005; Shigetomi, Bowser, Sofroniew, & Khakh, 2008]). One neuron per slice and 4–5 slices per mouse were recorded. Control experiments were performed in hippocampal slices transfected with viral vector (AAV2/5-GFAP-mCherry) or nontransfected slices stimulated with light. For astrocyte network loading, the holding potential was −70 mV. Intracellular solution containing GDPβS (20 mM), Evans Blue (5 μM), BAPTA (40 mM) and biocytin (0.1%) was used for astrocyte filling for 20–30 min ([in mM]: BAPTA-K_4 40, NaCl, 8, $MgCl_2$ 1, HEPES 10, GTP-tris salt 0.4, ATP-Na_2 2; pH = 7.3, with KOH). Slices were then fixed and biocytin was revealed by Alexa488-Streptavidin (Figure 4a), showing the wide area covered by the intracellular biocytin-loading, and confirming the broad downregulation of Ca^{2+} signals by BAPTA intracellular filling astrocytes (*cf.* Navarrete et al., 2012; Serrano, Haddjeri, Lacaille, & Robitaille, 2006).

2.5 | Calcium imaging

Microinjection of AAV2/5 in vivo resulted in reliable, high, and mosaic expression of membrane-tethered Lck-GCaMP6f within astrocytes throughout the hippocampus (Figure 1(b), cf.[Shigetomi et al., 2013]). Lck-GCaMP6f revealed the highly branched nature of astrocytes, labeling fine processes, termed microdomains, but less efficacy for proximal processes and cell soma, being revealed in a limited number of cells (*cf.* Haustein et al., 2014; Poskanzer & Yuste, 2016). Hence, in this study, the analysis of Ca^{2+} events in Lck-GCaMP6f astrocytes was mainly focused at microdomain levels (identified as functional microdomains; Agarwal et al., 2017; Mariotti et al., 2018; Srinivasan et al., 2015), including proximal processes when applicable. Imaging of Lck-GCaMP6f-astrocytes was performed with a two-photon laser scanning microscope (AxioImager M, LSM510, Zeiss Oberkochen, Germany) equipped with a pulsed red laser tuned at 900 nm (1.80 W, 1% of power; Spectra Physics Mai-Tai, Prairie Technologies, Sioux Falls, SD) for excitation of Lck-GCaMP6f. mCherry signal was acquired in a confocal laser scanning mode at 543 nm with a HeNe laser. Imaging was performed through a water immersion lens 40×/1.0 W Plan-Apochromat (Zeiss), with a field of view between 354 × 354 μm (for colocalization image), and 295 × 295 μm for acquisition at 1 Hz frame rate. Astrocyte imaging sessions consisted of 250–420 frames. Full-field photostimulation consisted in 1, 5, 10, and 20 s light pulses and low-frequency stimulation (LFS; 5 s @ 0.06 Hz, 1 min; λ = 473 nm) delivered by an external laser. Minor drift in the XY plane of image stacks was post hoc corrected using TurboReg (ImageJ plugin). In a subset of experiments, cyto-GCaMP6f was used to monitor Ca^{2+} signals in proximal processes and soma of the astrocytes using the acquisition parameters indicated above. ACFS was perfused with TTX (1 μM) for calcium imaging. Astrocytes showing both mCherry and GCaMP6f positive labeling were selected for analysis, and regions of interest (ROI) were selected from the GCaMP6f image. Detection of ROIs was performed with ImageJ in a semi-automated manner using the GECIquant program (Srinivasan et al., 2015) coming as an open source plugin. The mean ROI area was 11.06 ± 0.024 μm^2 (from 1 to 122 μm^2; included proximal processes when applicable). We identify ROIs corresponding to the soma (> 30 μm^2), and to processes (between 1 and 122 μm^2). The resulting detection was visually checked in every case. Custom-written software in MATLAB

(MATLAB R2016; Mathworks, Natick, MA) was used for computation of fluorescence (F) of each ROI. All pixels within each ROI were averaged to give a single time course $F[t]$. To compare relative changes in fluorescence between different ROIs, Ca^{2+} signal was analyzed as $\Delta F/F_0 = (F(t) - F_0)/(F_0)$, from now on termed $\Delta F/F$. F_0 represented baseline fluorescence of each ROI and defined as the average minimum fluorescence across prestimulus frames. ROIs with no Ca^{2+} signal changes during the entire recording (signals above five times SD of baseline) were discarded (14.67% for melanopsin, 19.34% for ChR2, and 21.15% for vector-transfected astrocytes; $p = 0.701$; one-way ANOVA, post hoc comparison with Dunn's test). For the case of *Ip3r2*$^{-/-}$ melanopsin-astrocytes, 51.82% of ROIs did not show activity and were discarded (wt-astrocytes vs. *Ip3r2*$^{-/-}$ astrocytes, $p = 0.012$; one-way ANOVA, post hoc comparison with Dunn's test; *cf*. Agarwal et al., 2017; Srinivasan et al., 2015). A Ca^{2+} event was defined as a signal that showed maximum values above three times SD of mean values of prestimulus frames, and for those superimposed events, maximum values above two times SD of the previous steady signal. Events with duration <2 frames were excluded. For each ROI, four parameters were analyzed: the frequency of events, amplitude, width, and onset. Onset was defined as the last point in the ΔF/F time course below 1 *SD* before a significant peak occurred. Width value was measured as the half prominence of each peak. Values were averaged across all astrocytes. From the onset histogram of Ca^{2+} events (Figure 1e), the "responding" ROIs were defined as those that showed at least one Ca^{2+} event in the first 20 s after light stimulation. All the Ca^{2+} traces were visually inspected to exclude the ROIs dominated by noise. Given the heterogeneity found in the amplitude of Ca^{2+} events, group segmentation was done using k-means MATLAB code. Hence, amplitude values were clustered in three mutually exclusive clusters in an unbiased mode based on feature similarity. ROIs showing at least one event in the first 60 s after stimulus, termed "active" ROIs, were analyzed (72.96% for melanopsin, and 58.22% for ChR2-transfected astrocytes; Supporting Information Figures S3 and S9). Frames with light artifacts were removed from the analysis.

For a particular set of experiments, astrocyte Ca^{2+} responses were evaluated by local application of DHPG (1 mM, 5 s), an agonist of group I metabotropic glutamate receptors, before and after intracellular loading of with GDPβS (20 mM). Experiments were performed in the presence of TTX (1 μM) and PPADS (30 μM), a nonselective P2 purinergic antagonist.

2.6 | Optogenetic stimulation

Full-field photostimulation was achieved through a diode-pumped solid-state blue laser with analog intensity control (473 nm, MBL-III-473, OptoEngine, LLC, Midvale, UT) coupled via SMA terminal to a 200 μm fiber (ThorLabs, Newton, NJ). In some experiments, photostimulation through the light path of the microscope objective was performed. Blue light pulses (7 mW/mm^2) at 10 Hz (50 ms light pulses) or continuous stimulation at variable durations (1, 5, 10, and 20 s) were delivered for two-photon Ca^{2+} experiments. No differences were found by light train or continuous stimulation and data were pooled together. Synaptic responses were evaluated by continuous light stimulation (1, 3, 5, 10, 20, and 60 s at 7 mW/mm^2), and by 10 Hz (50 ms light pulses) for 60 s. ChR2, melanopsin, and vector-transfected astrocytes were stimulated using the same light intensity (7 mW/mm^2), only for a subset of experiments showing in Figure 2g and Supporting Information Figure S5d, light intensity was changed.

2.7 | Immunohistochemistry

C57BL/6 wild-type mice or *Ip3r2*$^{-/-}$ mice transfected with viral vectors and C57BL/6 naïve mice were euthanized with sodium pentobarbital and transcardially perfused with PBS followed by ice-cold 4% paraformaldehyde in PBS. Brains were removed and postfixed overnight (o/n) at 4°C in the same fixative solution. Coronal brain slices of 50 μm were obtained in a VT1000S vibratome (Leica), collected as floating sections, and blocked for 1.5 hr at room temperature (RT) in a solution containing 0.3% Triton X-100 and 5% NGS in PBS. After blocking, sections were incubated (o/n; 4°C) with the following primary antibodies in a solution containing 0.3% Triton X-100 and 1% NGS in PBS: mouse anti-GFAP (1:500, Sigma, St. Louis, MO, RRID: AB_477010); rabbit anti-NeuN (1:500, Millipore, RRID:AB_2571567); mouse anti-NeuN (1:500, Millipore, Burlington, MA, RRID: AB_2298772); rabbit anti-s100 (1:100, Abcam, Cambridge, UK; RRID: AB_306716); rabbit anti-Iba1 (1:500, Wako, Huntley, IL, RRID: AB_839504). After three washes of 15 min. Each in PBS containing 0.3% Triton X-100, the floating sections were incubated with the specific Alexa conjugated antibodies in a PBS solution containing 0.3% Triton X-100 and 1% NGS for 2 hr at RT. The following antibodies were used: Alexa Fluor 488 Goat anti-mouse (1:200, Bioss Inc., Woburn, MA, RRID:AB_10892893); Pacific Blue Goat anti-rabbit (1:200, Thermo Fisher Scientific, Waltham, MA, RRID:AB_2539814); Alexa Fluor 647 Goat anti-rabbit (1:200, Thermo Fisher Scientific, RRID:AB_2535813); Alexa Fluor 488 Goat anti-rabbit (1:200, Thermo Fisher Scientific, RRID:AB_143165) and Alexa Fluor 405 Goat anti-rabbit (1:200, Thermo Fisher Scientific, RRID:AB_10680407). Before incubation with DAPI (1.5 μg/mL, Sigma-Aldrich) for 10 min, sections were washed (three times for 15 min each) in PBS containing 0.3% Triton X-100. Finally, sections were washed once in PBS and mounted in Vectashield antifading mounting medium (Vector Laboratories, Burlingame, CA). In order to study the potential microgliosis due to light stimulation in acute slices, 350 μm sections were illuminated during 20 s with the diode-pumped solid-state blue laser (473 nm) or kept in the dark for an equivalent amount of time. Subsequently, sections were fixed with ice-cold 4% paraformaldehyde in PBS (15 min) and then blocked o/n at 4°C in a solution containing 0.5 Triton X-100 and 5% NGS. Afterward, sections were incubated (24 h; 4°C) with rabbit anti-Iba1 (1:500, Wako, RRID:AB_839504). After four washes of 15 min each in PBS containing 0.5% Triton X-100, sections were incubated with the secondary antibody Alexa Fluor 488 Goat anti-rabbit (1:200, Thermo Fisher Scientific, RRID: AB_143165). Sections were washed (three times of 15 min each), incubated with DAPI (1.5 μg/mL, Sigma-Aldrich, St. Louis, MO) for 10 min, and mounted in Vectashield antifading mounting medium (Vector Laboratories). Sections were then stored at 4°C, and images were acquired on a Leica SP5 (Leica, Wetzlar, Germany) laser scanning confocal microscope.

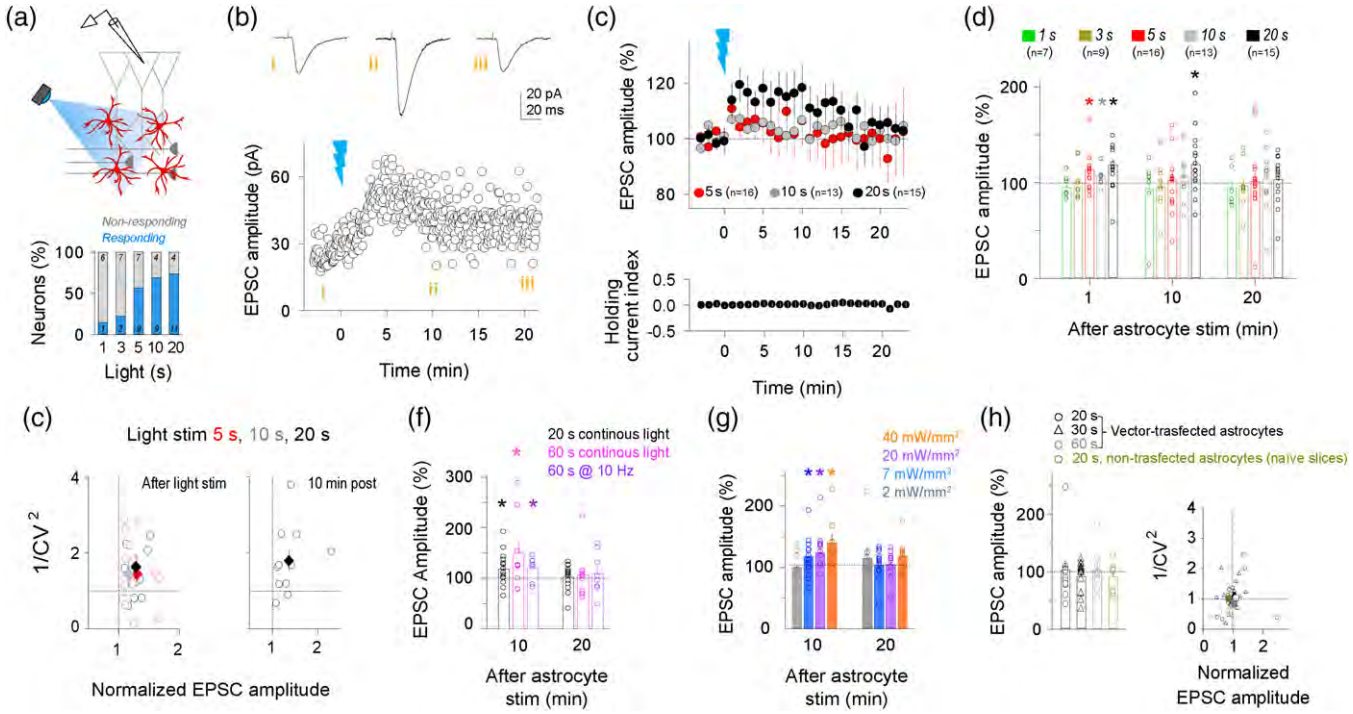

FIGURE 2 Light activation of melanopsin-transfected astrocytes induces enhancement of excitatory synaptic transmission in CA1 neurons. (a) *Top*: schematic drawing of the experimental design for synaptic recordings. *Bottom*: percentage of neurons showing synaptic changes after astrocyte light stimulation in blue. (b) Excitatory synaptic currents (EPSCs) before (i) and after (ii, iii), and a representative recording from CA1 neuron showing its EPSC amplitudes over time by 20 s of astrocyte light activation. Zero time indicates light pulse onset and astrocyte activation (blue beam denotes light stimulation). (c) *Top*: average of relative EPSC amplitude over time before and after astrocyte stimulation at different pulse durations. Zero time indicates light pulse (blue beam; 5 s, $n = 16$ neurons; 10 s, $n = 13$ neurons; 20 s, $n = 15$ neurons). *Bottom*: neuronal holding current index over time by 20 s of astrocyte photostimulation ($n = 15$ neurons). (d) Average of relative EPSC amplitude by light stimulation (1–20 s) at different time points of all recorded neurons. Values recorded at 10 min after 1 s (mean: 92.82%; SD: 36.36%; SEM: 13.74%; $n = 7$), 3 s (mean: 95.74%; SD: 26.26%; SEM: 8.75%; $n = 9$), 5 s (mean: 102.45%; SD: 31.83%; SEM: 7.96%; $n = 16$), 10 s (mean: 106.55%; SD: 23.79%; SEM: 6.59%; $n = 13$) and 20 s (mean: 118.52%; SD: 32.42%; SEM: 8.37%; $n = 15$); 5 s: 1 min ($p = 0.013$); 10 s: 1 min ($p = 0.021$); 20 s: 1 min ($p = 0.020$), 10 min ($p = 0.044$); paired *t* test. (e) Relative changes of the coefficient of variation (CV) after 1 min (5 s, $n = 9$; 10 s, $n = 9$; 20 s, $n = 11$) and 10 min of astrocyte stimulation (20 s, $n = 11$). (f) Relative changes of EPSC amplitude evoked by 20 s and longer pulses: continuous light stimulation for 60 s ($n = 9$; 10 min, $p = 0.020$), and 10 Hz for 60 s ($n = 8$; 10 min, $p = 0.039$). Note that longer pulses did not induce long-term synaptic changes, and no differences were found between 20 s versus longer light pulses. $p = 0.515$; one-way ANOVA, post hoc comparison with Dunn's test. $^*p < 0.05$. (g) Quantification of the EPSC amplitude changes induced by 20 s light pulses at different intensities recorded at 10 and 20 min after stimuli (10 min: 2 mW/mm^2, $n = 8$, $p = 0.912$; 7 mW/mm^2, $n = 15$, $p = 0.044$; 20 mW/mm^2, $n = 8$, $p = 0.035$; 40 mW/mm^2, $n = 9$, $p = 0.020$; paired *t* test). Note that no significant differences were found for synaptic potentiation evoked from 7 mW/mm^2 to 40 mW/mm^2 ($p = 0.354$; one-way ANOVA, post hoc comparison with Dunn's test). $^*p < 0.05$. (h) *Left*: relative changes of EPSC amplitude 10 min after light pulses induced by 20 s ($n = 15$), 30 s ($n = 15$), 60 s of light stimulation ($n = 8$) and nontransfected slices ($n = 8$ neurons). *Right*: Relative changes of the coefficient of variation (CV) measured at 10 min after of astrocyte stimulation. $p > 0.05$, paired *t* test. Data are shown as mean ± *SEM*

2.8 | Immunohistochemistry measurements and quantification

To study the colocalization of the mCherry reporter encoded in a viral vector with astrocytic and neuronal markers, both quantitative and qualitative measurements were carried out. Single optical sections (0.8 μm) obtained through a 63× 1.40 NA oil immersion objective were acquired, and the intensity correlation analysis (ICA) plugin of ImageJ was used for the quantitative colocalization analysis. Rolling ball background subtraction was applied before running the plugin, and the Pearson's correlation coefficient yielded by the software was considered for analysis. For qualitative colocalization analysis, *z*-stack images (10 μm thickness) obtained through a 40× 1.25NA oil immersion objective were collected for visual identification of mCherry positive astrocytes. Furthermore, s100 and NeuN were used as astrocytic and neuronal markers, respectively, in order to quantify the number of double-positive cells. To investigate the potential microgliosis elicited by light stimulation or viral transfection, Iba1 labeled sections were imaged. Maximal projections of z-stacks (10 μm thickness) obtained through a 40× 1.25NA oil immersion objective were made, and single Iba1$^+$ cells were unequivocally recognized by DAPI counterstaining. In order to examine the distribution of mCherry fluorescence along the astrocytic processes, we used single optical sections (0.8 μm) collected through a 63× 1.40 NA oil immersion objective. Line plots were drawn from perisomatic regions (defined by the outline of DAPI labeling) to the distal end of astrocytic processes. To quantify the fluorescence in somatic regions we employed the first

0.5 μm of each line plot. The region comprised between 10 and 20 μm was used to quantify the fluorescence in astrocytic processes. To estimate the fluorescence in astrocytic endfeet, we traced line plots along noticeable endfeet of astrocytic processes. For the analysis of mCherry expression levels yielded by the different AAV vectors, we used Maximal projections of z-stacks (8 μm thickness) obtained with a 63× 1.40 NA oil immersion objective (digital zoom = 2×). After thresholding the images, a binary mask was rendered. The mask was superimposed over background subtracted images and the fluorescence values were collected as mean gray values for different astrocytes transfected with each viral vector. Comparisons among the different treatments and conditions were made and the specific statistical test is indicated in figure legends. To study the potential astrogliosis induced by viral injections, GFAP labeled sections were imaged through a 40× 1.25NA oil immersion objective. Z-stack images (10 μm thickness) were thresholded and the binary mask was applied over the background subtracted images for quantifications.

2.9 | Behavioral experiments

Behavioral experiments were performed in the morning (before 3 p.m.). To evaluate cognitive performance without an intrinsic stress *Novel Object Location* (NOL) test was used. The memory test consisted of three phases: habituation, sample (acquisition), and test trials. Mice (6–8 weeks) were first habituated individually to an empty open-field box (L, W, H: 50 × 40 × 40 cm) for 30 min. Next day, a sample trial (object exposure) was performed consisting on placing the mouse into the box for 10 min. After a delay (retention period of 30 min), the mouse was back in the box for the test trial. Light protocol (LFS: 5 s light ON, 10 light OFF) was applied during 3 min during the sample trial. The test trial consisted of switching the location of one of the objects (novel location of the displaced object). A recognition index was calculated by dividing the total time spent exploring the displaced object by the total time exploring both objects during the test trial. The animals' behavior was scored by an observer blind to the treatment conditions.

2.10 | In vivo light protocol

To optogenetically activate astrocytes, blue light (473 nm) was bilaterally delivered through two 100 μm thick optic fibers ending in a ceramic ferrule (Thorlabs) that were implanted and attached to the patch cords. Light was delivered for 3 min (5 s light ON; 10 s light OFF cycles).

2.11 | Drugs and chemicals

D-(−)-2-Amino-5-phosphonopentanoic acid (D-AP5), (S)-(+)-α-Amino-4-carboxy-2-methylbenzeneacetic acid (LY367385), MRS2179 tetrasodium salt (0900), Evans Blue tetrasodium salt (0845), SCH58261 (227010), (S)-3,5-dihydroxyphenylglycine (DHPG), and pyridoxal phosphate-6-azophenyl-2′,4′-disulfonic acid tetrasodium salt (PPADS; 0625) were purchased from Tocris Bioscience. Tetrodotoxin (TTX) was purchased from Alomone Labs (Jerusalem, Israel). GAP-26 was purchased from Apexbio (A1044). Light chain Tetanus toxin (TeTXLc) was purchased from List Biological Laboratories, Inc. (Campbell, CA). All other drugs, including Guanosine 5′-[β-thio]diphosphate (GDPβS trilithium salt; G7637), were purchased from Sigma-Aldrich.

2.12 | Statistical analysis

Data are expressed as the mean ± standard error of the mean (*SEM*). For Figures 2d, 3g, and 5h standard deviation (*SD*) was provided. Statistical analyses were performed using Sigmaplot 13.0 and MATLAB. Normality test was performed before applying statistical comparisons which were made using nonparametric Rank-sum test and parametric Student's *t* tests, one-way ANOVA or two-way ANOVA when appropriate, and followed by post hoc comparison with Tukey–Kramer or Dunn's tests as deemed appropriate. Two-tailed, unpaired or paired test was used for comparisons unless indicated. *p* value and test employed are reported in the text and/or figures legends. Statistical differences were established with $p < 0.05$ (*), $p < 0.01$ (**), and $p < 0.001$ (***; #). Randomization was not employed. Sample size for whole-cell recording experiments was based on values previously found sufficient to detect significant changes in hippocampal synaptic strength in the past studies from the lab.

All relevant data or codes are available from the authors.

3 | RESULTS

3.1 | Melanopsin: A new optical tool to control astrocyte Ca^{2+} signaling

In order to investigate the ability of melanopsin to modulate astrocyte Ca^{2+} signaling, the gene for the opsin (*Opn4*-human melanopsin) was fused to the glial fibrillary acidic protein (*Gfap*) promoter and expressed in astrocytes following an adeno-associated virus (AAV)-based strategy (AAV2/5-Gfap-melanopsin-mCherry; Figure 1a and b). To monitor Ca^{2+} signals, the membrane-targeted genetically encoded Ca^{2+} indicator (GECI) Lck-GCaMP6f was selectively co-expressed with melanopsin in hippocampal astrocytes (Figure 1a–c; see Methods). Lck-GCaMP6f revealed the highly branched nature of astrocytes, labeling fine processes (Shigetomi et al., 2013), where the analysis of Ca^{2+} events was focused. Some key features of melanopsin transfection were analyzed (Supporting Information Figures S1 and S2), showing the specifically targeted expression in astrocytes, and the absence of measurable astrocyte reactivity caused by either viral transfection (Shigetomi et al., 2013) or melanopsin expression (Supporting Information Figure S1a,b). For Ca^{2+} imaging experiments, only astrocytes showing both mCherry-melanopsin and GCaMP6f labeling were considered for the analysis. After blue light (473 nm) stimulation, hippocampal astrocytes showed robust Ca^{2+} increases in fine processes and soma (Figure 1c–g). The analysis of Ca^{2+} signals indicated that light pulses of different durations (1, 5, 10, and 20 s) increased the frequency of Ca^{2+} events per region of interest (ROI) at the soma (Figure 1f) and microdomains (Figure 1c–e, g), without changing the amplitude of Ca^{2+} events in each ROI (Figure 1f–g). Additionally, the duration of Ca^{2+} events at microdomains was reduced after longer light stimuli (1 s: 4.76 ± 0.2 s; 20 s: 4.34 ± 0.12; $p < 0.001$;

Figure 1f). Considering the limited number of cells showing Lck-GCaMP6f expression at the soma (Haustein et al., 2014; Poskanzer & Yuste, 2016; Shigetomi et al., 2013), we focused on Ca^{2+} events at astrocytic branches. Although different light pulses evoked similar maximum response onset delay (~3 s after the end of stimulus; Figure 1e), we found that longer light stimuli increased the number of ROIs showing Ca^{2+} events (Figure 1e). In order to investigate the particular features of melanopsin-driven Ca^{2+} responses, we analyzed Ca^{2+} events occurring up to 60 s after light stimulus, based on the prestimulus amplitude values were classified in three groups (active ROIs, see Methods; Supporting Information Figure S3). ROIs with small Ca^{2+} event amplitude only showed further Ca^{2+} increases following 20 s light pulses, but they significantly increased their oscillation frequency at all tested light pulses. Additionally, a reduced Ca^{2+} event duration was observed by 10 and 20 s light pulses. Interestingly, ROIs with higher Ca^{2+} signals in resting conditions were insensitive to further increase in amplitude, and only longer light pulses evoked an increase in the event frequency related with a reduced duration of the events (Supporting Information Figure S3b). To confirm whether melanopsin could also stimulate Ca^{2+} signals at the soma levels, a subset of experiments was performed using cyto-GCaMP6f (AAV2/5-Gfap-cyto-GCaMP6f) that were co-transfected with melanopsin into astrocytes. A 20 s light stimulation evoked an increase in the frequency of somatic Ca^{2+} peaks, but no significant changes in the amplitude or duration of the Ca^{2+} events were found, similar to data found with Lck-GCaMP6f (Supporting Information Figure S3c).

Melanopsin activation was also monitored by whole-cell recordings from mCherry-expressing astrocytes showing weak outward currents in response to blue light (Supporting Information Figure S4a, b). It has been recently reported that melanopsin activates Ca^{2+}-dependent K^+ channels in cortical neurons (McGregor, Becamel, Marin, & Andrade, 2016). Consistent with these data, we found that light-induced astrocytic outward currents were reduced in presence of apamin (100 nM), a selective blocker of Ca^{2+}-dependent K^+ channels (Supporting Information Figure S4c). Altogether, these data show that the ectopic expression of melanopsin in hippocampal astrocytes was competent to trigger intracellular Ca^{2+} signals.

3.2 | Light activation of melanopsin-transfected astrocytes induces short-term potentiation of synaptic plasticity

Astrocyte activity has been found to influence synaptic physiology, including regulation of synaptic transmission and plasticity (Araque et al., 2014). Hence, we next investigated whether melanopsin-driven astrocyte Ca^{2+} signals had an impact on neuronal activity by recording excitatory postsynaptic currents (EPSCs) from pyramidal CA1 neurons (Figure 2a and b). Astrocyte Ca^{2+} signals were successfully induced at 1 s light stimulation (Figure 1g and Supporting Information Figure S3); however, no changes in synaptic transmission were found by short light pulses, that is, 1 and 3 s (Figure 2d). Only after ≥5 s light stimulation, a transient increase of synaptic strength was observed (Figure 2c and d). We found that longer light pulses (20 s) evoked transient EPSC potentiation that last over 10 min after astrocyte stimulation (118.52 ± 8.37% from baseline at 10 min after 20 s light stim; n = 15; p = 0.044; Figure 2b–d), without modifying the holding current (Figure 2c), discarding a depolarization of postsynaptic neuron. We further analyzed the synaptic locus of the short-term synaptic changes calculating the coefficient of variation (CV) of EPSCs, which measures the trial-to-trial variability of the synaptic responses (see Methods), and indicated presynaptic mechanisms underlying the melanopsin-driven short-term plasticity (Figure 2e). Accordingly, the miniature synaptic responses (mEPSCs) showed a transient increase in frequency, but no changes in mEPSC amplitude (Supporting Information Figure S5a and b). In addition, whole cell recordings in astrocytes were performed and the astrocytic glutamate transporter-dependent currents monitored (Devaraju, Sun, Myers, Lauderdale, & Fiacco, 2013), showing an increase in the amplitude of peak current after light stimulation (Supporting Information Figure S5c). Although a partial contribution of postsynaptic activity cannot be totally excluded given the reported actions of astrocyte signaling that increase the trafficking of AMPA receptors to the synapses (Boue-Grabot & Pankratov, 2017; Gordon et al., 2005; Lalo et al., 2014), our data suggest that glutamatergic synaptic transmission was mainly enhanced via presynaptic mechanisms after melanopsin-astrocyte stimulation.

To evaluate whether even longer light stimuli could further extend synaptic modulation, 60 s continuous light pulses and 10 Hz (50 ms light pulses) during 60 s were delivered to melanopsin-astrocytes. After those light protocols both the amplitude and duration of synaptic modulation were not further enhanced (Figure 2f). We next analyzed whether synaptic potentiation was tuned by different light intensities (range from 0.15 to 40 mW/mm^2). While the area of astrocytic melanopsin-evoked membrane currents displayed a linear increase with light intensity Supporting Information Figure S5d), the melanopsin-induced synaptic modulation was observed for intensities ≥7 mW/mm^2 (note that 7 mW/mm^2 were the reference intensity used in this study) (Figure 2g). Remarkably, no additional enhancement of EPSC potentiation was observed at higher intensities (7 mW/mm^2 vs. 40 mW/mm^2; p = 0.354; Figure 2g).

A reporter vector (AAV2/5-GFAP-mCherry) was expressed into astrocytes and analyzed. Light stimulation failed to induce both astrocyte Ca^{2+} transients and synaptic modulation in the reporter transfected animals (97.31 ± 11.64% from baseline after 20 s light stimulation; n = 15; p = 0.169), which excluded that viral transfection or blue light might per se contribute to the observed changes (Figure 2h, and Supporting Information Figure S6).

Nowadays ChR2 is the opsin commonly used for astrocyte activation (Gourine et al., 2010; Pelluru et al., 2016; Perea et al., 2014; Sasaki et al., 2012; Shen, Nikolic, Meunier, Pfrieger, & Audinat, 2017). Therefore, we analyzed the features and consequences of using ChR2 for astrocyte activation under similar light conditions applied to melanopsin. Analogous viral strategy was followed (AAV2/5-GFAP-ChR2-mCherry), and Ca^{2+} signals were monitored by selective expression of Lck-GCamp6f (Figure 3a). We found that light stimulation had a modest activation of Ca^{2+} signals at astrocytic processes (Figure 3b–d). The frequency of Ca^{2+} events per ROI was increased after 10 and 20 s light stimulation (Figure 3c; Supporting Information Figure S7a), but unchanged after short light pulses (1 and 5 s; Figure 3c). Additionally, no significant changes were found in the amplitude or width of the Ca^{2+} events at microdomains level (Supporting Information Figure S7b). In a

subset of experiments, somatic Ca^{2+} events were recorded by expression cyto-GCaMP6f in astrocytes, which showed a clear increase in their frequency, but no changes were found in the Ca^{2+} event amplitude (Supporting Information Figure S7c). Patch-clamp recordings showed that light stimulation evoked robust inward currents in transfected-astrocytes, confirming the functional expression of ChR2 (Lin, 2011; Supporting Information Figure S7d). Additionally, ChR2-astrocyte stimulation was competent to modulate synaptic transmission in CA1 neurons (Figure 3e, g). A brief transient synaptic boost was observed after 5 s light; however, higher and sustained synaptic modulation (at least 20 min post stim) was found by longer astrocyte stimuli (154.05 ± 12.99% from baseline for 20 s light pulse; n = 13; p = 0.008; Figure 3f, g), which showed presynaptic mechanisms of action (Supporting Information Figure S7f). The different sensitivity showed by melanopsin and ChR2 for Ca^{2+} signals were not due at least to diverse intensity patterns of reporter expression (Supporting Information Figure S7g, h), but it might be related to the capability of these opsins to engage intracellular Ca^{2+} signals. Indeed, melanopsin had a higher efficacy than ChR2 to stimulate Ca^{2+} signals both at the soma and microdomains, even at short pulses (Figure 3h, i). However, the impact on synaptic transmission by ChR2-astrocyte stimulation was present for longer periods (Figure 3j). Considering the weaker Ca^{2+} responses and the sustained synaptic changes evoked by ChR2-astrocytes, these data suggest a narrow window of ChR2 to precisely control astrocyte-to-neuron signaling.

3.3 | Melanopsin recruits astrocyte G-protein and Ca^{2+}-dependent pathways

Astrocyte neuromodulation by means of different substrates is based on Ca^{2+}-dependent and independent mechanisms (Bazargani & Attwell, 2016). In order to confirm the causal relationship between synaptic potentiation and melanopsin-induced astrocytic Ca^{2+}, the downregulation of Ca^{2+} signals was pursued. Based on the reported melanopsin G-protein activity (Panda et al., 2005), a competitive blocker of G-proteins GDPβS (20 mM) was intracellularly loaded into melanopsin-expressing astrocytes by the recording pipette and dialyzed into astrocyte network (Figure 4a). The efficacy of GDPβS action was confirmed by the absence of astrocyte Ca^{2+} responses to DHPG (1 mM), a selective agonist of group I metabotropic glutamate receptors (mGluRs; Supporting Information Figure S8). After 20–30 min of GDPβS-loading, light stimulation failed to induce synaptic enhancement (98.58 ± 9.20% from baseline; n = 6; p = 0.820; Figure 4b). Additionally, astrocyte Ca^{2+} was blocked by intracellular loading of the Ca^{2+} chelator BAPTA (40 mM) into the astrocyte syncytium. Under these conditions, astrocyte stimulation failed to evoke changes in EPSC strength (97.59 ± 9.99% from baseline; n = 5; p = 0.885; Figure 4b), confirming the contribution of the astrocyte G-protein and Ca^{2+}-dependent pathways to the observed synaptic potentiation.

To overcome limitations associated with pharmacological manipulations and considering that melanopsin activation induces Ca^{2+} release from IP3-sensitive intracellular stores in ganglion cells (Peinado, Osorno, Gomez Mdel, & Nasi, 2015), we evaluated melanopsin actions in the *Ip3r2*$^{-/-}$ mice (X. Li et al., 2005), which show a weakened Ca^{2+} signaling in astrocytes (Agarwal et al., 2017; Navarrete et al., 2012; Sherwood et al., 2017; Srinivasan et al., 2015). *Ip3r2*$^{-/-}$ mice were transfected with viral vectors containing melanopsin and Lck-GCaMP6f, and the spontaneous and light-evoked Ca^{2+} transients were evaluated (Figure 5a). In line with previous results (Agarwal et al., 2017; Haustein et al., 2014; Srinivasan et al., 2015), a downregulated Ca^{2+} signaling in resting conditions was observed in melanopsin-*Ip3r2*$^{-/-}$ astrocytes (Figure 5b–e). After light stimulation, melanopsin was unable to modify the Ca^{2+} event properties in the astrocyte processes at any light pulse tested (Figure 5c and d). To evaluate whether melanopsin could stimulate Ca^{2+} signals at the astrocyte soma, where IP3-sensitive stores play a major role, cyto-GCaMP6f was expressed in *Ip3r2*$^{-/-}$ astrocytes. However, light stimulation failed to evoke Ca^{2+} signals at the soma (Figure 5e), suggesting the specific IP3 signaling pathway engaged by melanopsin. Likewise, no EPSC changes were found after astrocyte stimulation (Figure 5f–i). Therefore, these data confirm that melanopsin-mediated synaptic enhancement was driven by the astrocytic boosting of intracellular IP3-dependent Ca^{2+} pathways.

3.4 | Melanopsin-evoked purinergic signaling triggers synaptic plasticity

We next evaluated the gliotransmitters and receptors involved in the synaptic responses evoked by melanopsin-astrocyte signaling. EPSC potentiation was present in the presence of LY367385 (100 μM), a selective blocker of mGluR1a subtype (Figure 6a and b; n = 8 neurons; p = 0.046), which has been related with astrocyte-evoked synaptic modulation in the hippocampus (Gomez-Gonzalo et al., 2015; Perea & Araque, 2007) and other brain areas (Martin, Bajo-Graneras, Moratalla, Perea, & Araque, 2015; Perea et al., 2014; Sasaki et al., 2012). Conversely, synaptic modulation was sensitive to purinergic signaling (Di Castro et al., 2011; Gourine et al., 2010; Lalo, Palygin, Verkhratsky, Grant, & Pankratov, 2016; Panatier et al., 2011; Pougnet et al., 2014; Tan et al., 2017), and was abolished by MRS2179 (10 μM; 96.40 ± 6.16% from baseline; n = 12 neurons; p = 0.571), the purinergic $P2Y_1$ receptor antagonist, SCH58261 (Figure 6a and b; 10 μM; 100.86 ± 10.51% from baseline; n = 10 neurons; p = 0.695), the adenosine $A2_A$ receptor antagonist, previously found to stimulate synaptic transmission; but synaptic enhancement was still present after blockage of P2X receptors with PPADS (Figure 6b; 10 μM; 143.57 ± 18.75% from baseline; n = 10 neurons; p = 0.045). Therefore, these data suggested that ATP/Adenosine (Ado) released by melanopsin-astrocytes were involved in the synaptic boost. On the other hand, the EPSC modulation evoked by ChR2-transfected astrocytes was abolished by LY 367385 (n = 11 neurons; p = 0.899) and MRS 2179 (n = 8 neurons; p = 0.491), but insensitive to the purinergic adenosine $A2_A$ receptor antagonist (Figure 6b; n = 8 neurons; p = 0.013). These results indicated that while melanopsin triggered a purinergic-mediated synaptic modulation, the ChR2-induced potentiation required the action of both glutamatergic and purinergic signaling. In order to confirm whether melanopsin might stimulate glutamate release, we analyzed the NMDA-dependent slow inward currents (SIC), which has been related to glutamate released from astrocytes (Perea & Araque, 2005; Shigetomi et al., 2008). Following melanopsin-astrocyte activation, CA1 neurons displayed a significant increase in

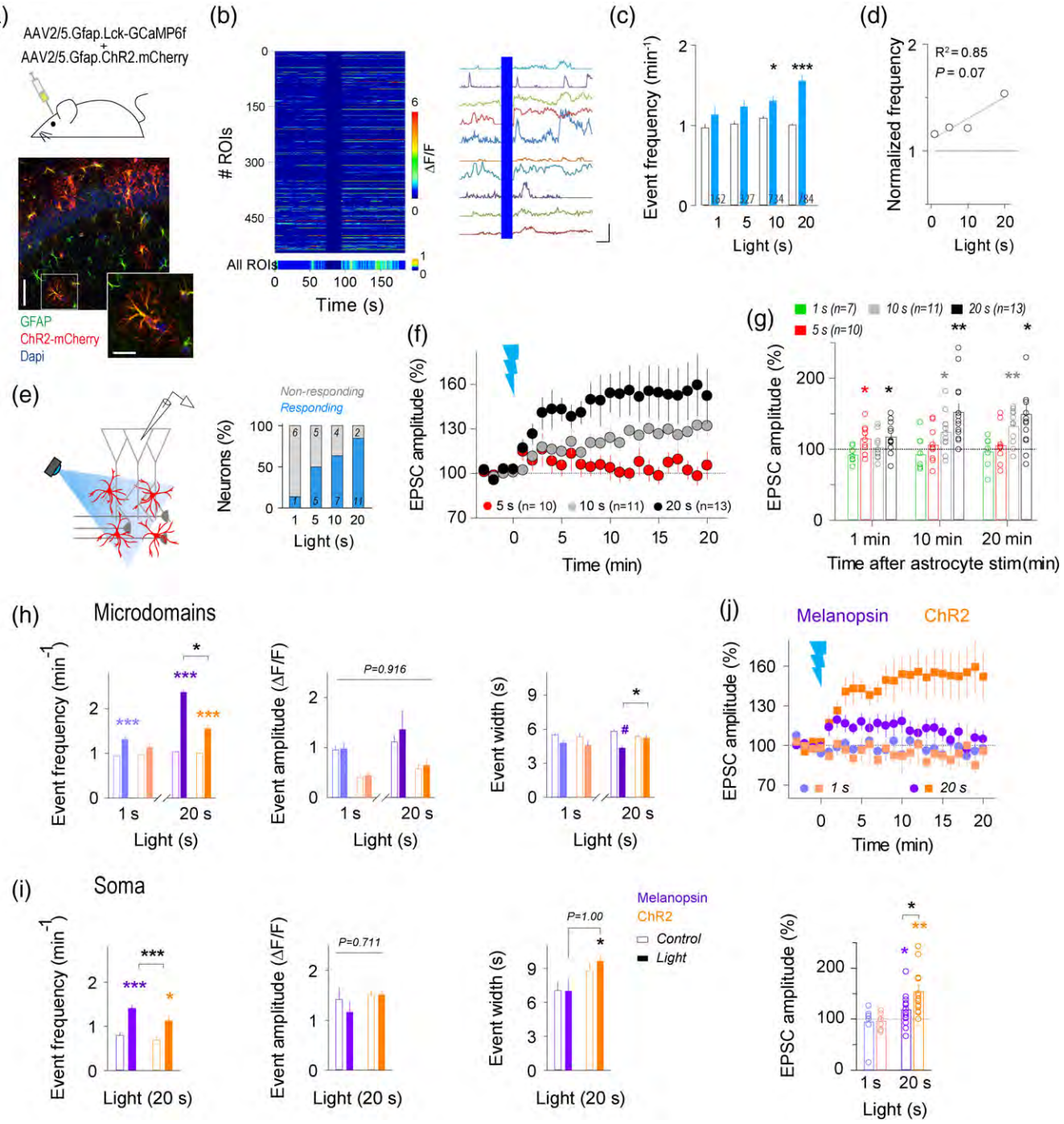

FIGURE 3 Selective ChR2 activation of hippocampal astrocytes stimulates Ca^{2+} signaling and synaptic changes. (a) *Top*: viral transfection of AAV2/5-Gfap-Lck.GCaMP6f and AAV2/5-Gfap-ChR2-mCherry in hippocampus. *Bottom*: immunocytochemical localization of ChR2-mCherry (red), GFAP (green), and DAPI nuclei (blue) in hippocampal slices. Inset of high magnification of representative astrocyte. Scale bar = 50 and 20 μm, respectively. (b) *Left*: representative raster plot of microdomain activity, color coded according to fluorescence change (top, n = 500), and average microdomain population activity versus time (bottom, n = 784). *Right*: representative intensity of Ca^{2+} signals versus time evoked by ChR2 light stimulation (20 s; blue bar). Scale bar = 1.5 $\Delta F/F$, 25 s. (c) Analysis of microdomain Ca^{2+} fluctuation properties showing mean responses for event frequency (1 s, n = 162 out of 237 (62.35%); 5 s, n = 327 out of 451 (72.50%); 10 s, n = 734 out of 851 (86.25%); 20 s, n = 784 out of 821 (95.49%); 25 slices from five mice). Resting versus light 10 s, p = 0.025; 20 s, p < 0.001. Two-way ANOVA analysis, post hoc comparison with Tukey–Kramer test; * p < 0.05; *** p < 0.001. (d) Normalized changes in frequency of microdomain events to resting conditions and linear fitting between different stimuli conditions. (e) Schematic drawing of experimental design for synaptic recordings and percentage of neurons showing synaptic changes after ChR2-astrocyte stimulation. (f) Average of relative changes of EPSC amplitude over time after astrocyte stimulation by different light conditions (1 s, n = 7; 5 s, n = 10; 10 s, n = 11; 20 s, n = 13). Zero time indicates light pulse (blue beam). (g) Relative changes of EPSC amplitude by ChR2 stimulation at different time points. Values recorded at 10 min after ChR2-light stim of 1 s (mean: 96.72%; SD: 24.21%; SEM: 9.15%; n = 7), 5 s (mean: 105.62%; SD: 24.53%; SEM: 7.76%; n = 10), 10 s (mean: 123.97%; SD: 28.09%; SEM: 8.47%; n = 11) and 20 s (mean: 151.95%; SD: 43.74%; SEM: 12.13%; n = 13). 5 s: 1 min (p = 0.039); 10 s: 10 min (p = 0.018), 20 min (p = 0.001); 20 s: 1 min (p = 0.012), 10 min (p = 0.001), 20 min (p = 0.008). *p < 0.05, **p < 0.01; paired t-test. (h) Analysis of Ca^{2+} fluctuation properties induced by

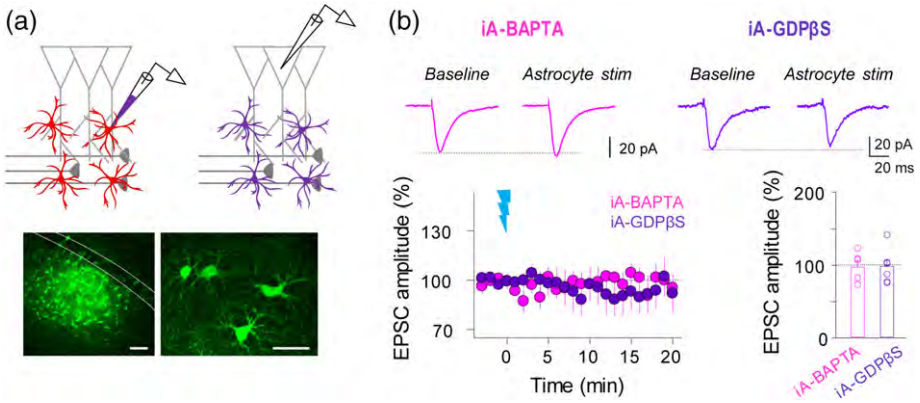

FIGURE 4 Melanopsin triggers G-protein-dependent Ca^{2+} signaling in astrocytes. (a) *Top*, schematic drawing of intracellular loading of astrocyte network with BAPTA or GDPβS by the recording pipette. *Bottom*, maximal projection confocal image of the astrocytic syncytium revealed by biocytin-loading via whole-cell astrocyte recording in the *stratum radiatum*, and high magnification of representative loaded astrocytes. Scale bar = 50 μm and 25 μm, respectively. (b) Representative EPSCs responses before and after 20 s of melanopsin-astrocyte stimulation in control and after astrocyte BAPTA or GDPβS-loading. Average of relative changes of EPSC amplitude over time (blue beam denotes 20 s light stimulation); and histograms of relative changes of EPSC amplitude recorded 10 min after astrocyte stimulation (BAPTA, 98.58 ± 9.20%; $n = 5$; $p = 0.410$; GDPβS, 97.59 ± 10.00%; $n = 6$; $p = 0.443$). $p > 0.05$; paired t-test. Data are shown as mean ± *SEM*

the SIC frequency (Figure 6c–e; 2.46 ± 0.77; $n = 12$; $p = 0.007$), indicating the ability of melanopsin to trigger the release of both transmitters glutamate and ATP/Adenosine.

Gliotransmission can be achieved by vesicular-dependent and independent mechanisms (Bazargani & Attwell, 2016), involving regulated exocytosis (Araque et al., 2014), and connexin/pannexin hemichannels (Bennett et al., 2012). Following the intracellular loading of astrocytes with Evans blue (5 μM), which blocks both the vesicular glutamate transporter (VGLUT) function (Eriksen et al., 2016; Goh et al., 2011; Sanchez-Mendoza et al., 2017), and the nucleotide transporters (VNUTs) that actively accumulate ATP into vesicles (Geisler et al., 2013; Oya et al., 2013; Sakamoto et al., 2014), light stimulation failed to induce astrocyte-mediated increase of SIC frequency (Figure 6e; 0.68 ± 0.31; $n = 8$; $p = 0.677$), as well as blocked the transient synaptic potentiation (Figure 6f, 99.96 ± 7.24%; $n = 8$ neurons; $p = 0.996$). Conversely, the blockage of connexin-hemichannels and gap junctions by bath application of the connexin 43 mimetic peptide Gap26 (100 μM; Karpuk, Burkovetskaya, Fritz, Angle, & Kielian, 2011; Roux et al., 2015) did not prevent both the increase of SIC frequency (Figure 6(e), 1.95 ± 0.52; $n = 8$; $p = 0.016$), and synaptic potentiation evoked by melanopsin-astrocyte stimulation (Figure 6f, 126.33 ± 14.73%; $n = 8$; $p = 0.010$). Additionally, the light chain of tetanus toxin (TeTxLC) that cleaves the vesicle-associated synaptobrevin-2 required for exocytosis was included into the astrocytic recording pipette, and synaptic responses were analyzed before and after light stimulation. The presence of TeTxLC (1 μM) into astrocytes blocked the melanopsin-induced synaptic potentiation in neighboring neurons (Figure 5f, 107.39 ± 30.09%; $n = 8$; $p = 0.547$). Altogether, these data support the contribution of vesicular-dependent pathways of gliotransmitter release (Henneberger, Papouin, Oliet, & Rusakov, 2010; Jourdain et al., 2007; Min & Nevian, 2012; Perea & Araque, 2007; Schwarz, Zhao, Kirchhoff, & Bruns, 2017) to the neuronal modulation triggered by melanopsin activation.

3.5 | Low-frequency light activation of melanopsin-astrocytes triggers hippocampal long-term plasticity and enhances memory performance in vivo

Astrocytes displayed low frequency spontaneous oscillatory activity that could be enhanced after melanopsin light activation (from 1.13 ± 0.024 in basal conditions to 1.78 ± 0.048 min^{-1} after 5 s light pulse; ~0.03 Hz; $p < 0.001$; Figure 1g). We then tested whether tuning astrocyte activity within this low-frequency range might engage different forms of Ca^{2+} signaling and synaptic plasticity. Astrocytes stimulated at low frequency (low-frequency stimulation protocol, LFS; 5 s light pulse @ 0.06 Hz, 1 min; Supporting Information Figure S9a and b) showed a robust enhancement of the Ca^{2+} signals located at the astrocytic microdomains (Figure 7a and b). Based on the prestimulus amplitude value of Ca^{2+} events (see Methods; Supporting Information Figure S9c), ROIs showed a systematic increase in the frequency

melanopsin (purple) and ChR2 (orange) in microdomains at 1 and 20 s light stimulation showing mean responses for event frequency, amplitude and width. Note that light stimulation of melanopsin at 1 s boosted the Ca^{2+} event frequency, while ChR2 failed to evoke changes; 20 s light pulse evoked higher mean frequency in melanopsin- than ChR2-transfected astrocytes ($p = 0.021$). Additionally, after 20 s light pulse melanopsin, but not ChR2, induced shorter Ca^{2+} events ($p = 0.045$). Two-way ANOVA, post hoc comparison with Tukey–Kramer test. (i) Somatic Ca^{2+} fluctuation properties of cyto-GCaMP6f-melanopsin (purple) and cyto-GCaMP6f-ChR2 (orange) expressing astrocytes induced by 20 s light pulse. Changes in event frequency were higher for melanopsin ($p < 0.001$) than ChR2-transfected ($p = 0.01$) astrocytes, while amplitude and width of Ca^{2+} events did not show differences ($p = 0.711$ and $p = 1.00$; respectively). Two-way ANOVA, post hoc comparison with Tukey–Kramer test. (j) *Top*: relative changes of EPSC amplitude over time by 1 and 20 s light stimulation of melanopsin-astrocytes and ChR2-astrocytes. Zero time indicates light pulse (blue beam). *Bottom*: mean values of EPSC amplitude at 10 min after light stimulation of melanopsin- and ChR2-astrocytes. Differences were found between 20 s light pulses. $p = 0.014$; unpaired *t* test. *$p < 0.05$; ***, #$p < 0.001$. Data are shown as mean ± *SEM*

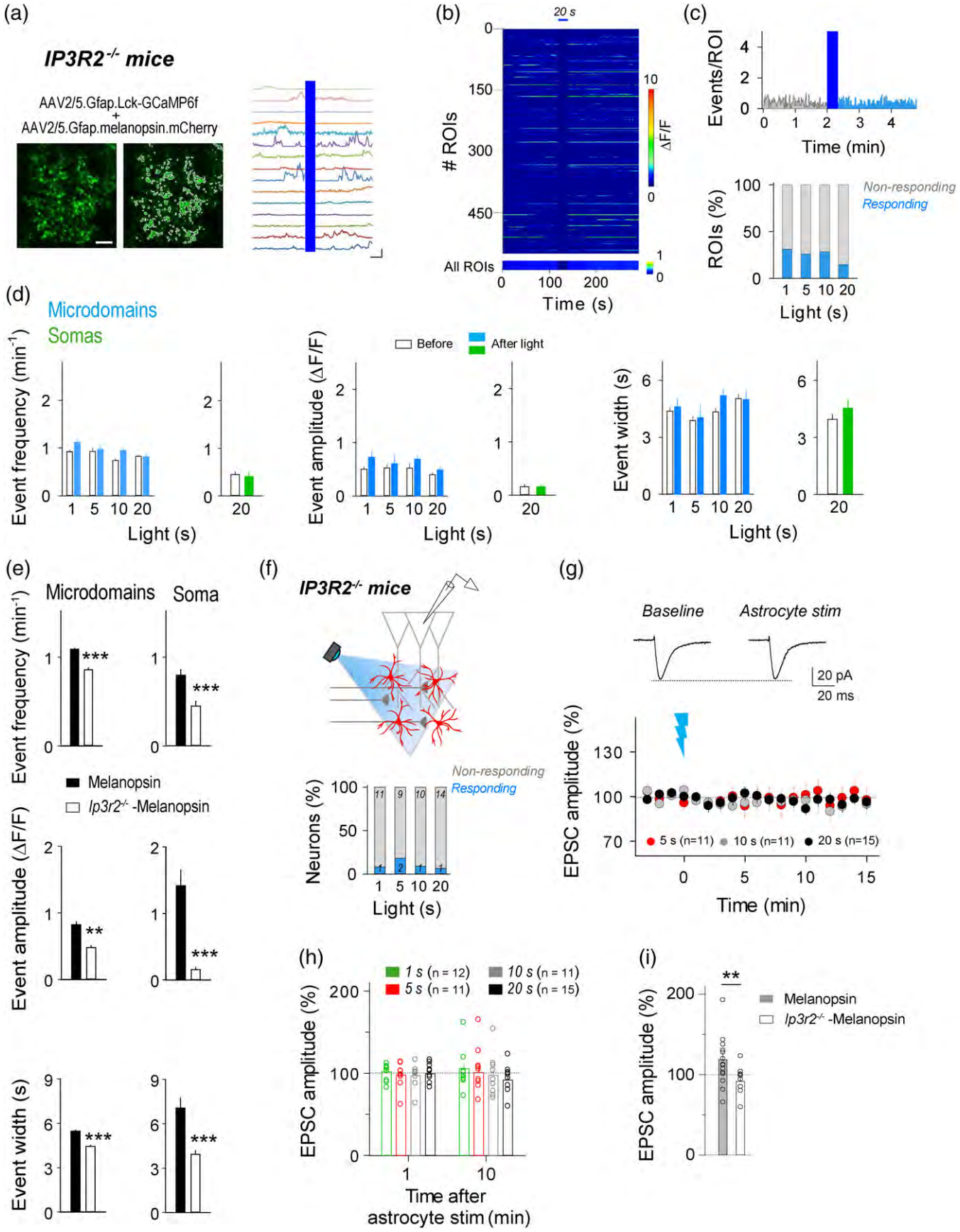

FIGURE 5 Melanopsin triggers IP3-dependent Ca^{2+} signals in astrocytes. (a) Image of an astrocyte from Gfap.Lck-GCaMP6f *Ip3r2*$^{-/-}$ mouse, and the same astrocyte showing the selected microdomains identified by GECIquant on ImageJ mask generator. *Right:* representative intensity Ca^{2+} signals versus time evoked by melanopsin light stimulation (20 s; blue bar) in *Ip3r2*$^{-/-}$ astrocytes. Scale bar, 10 μm; 3 Δ*F*/*F*, 25 s.

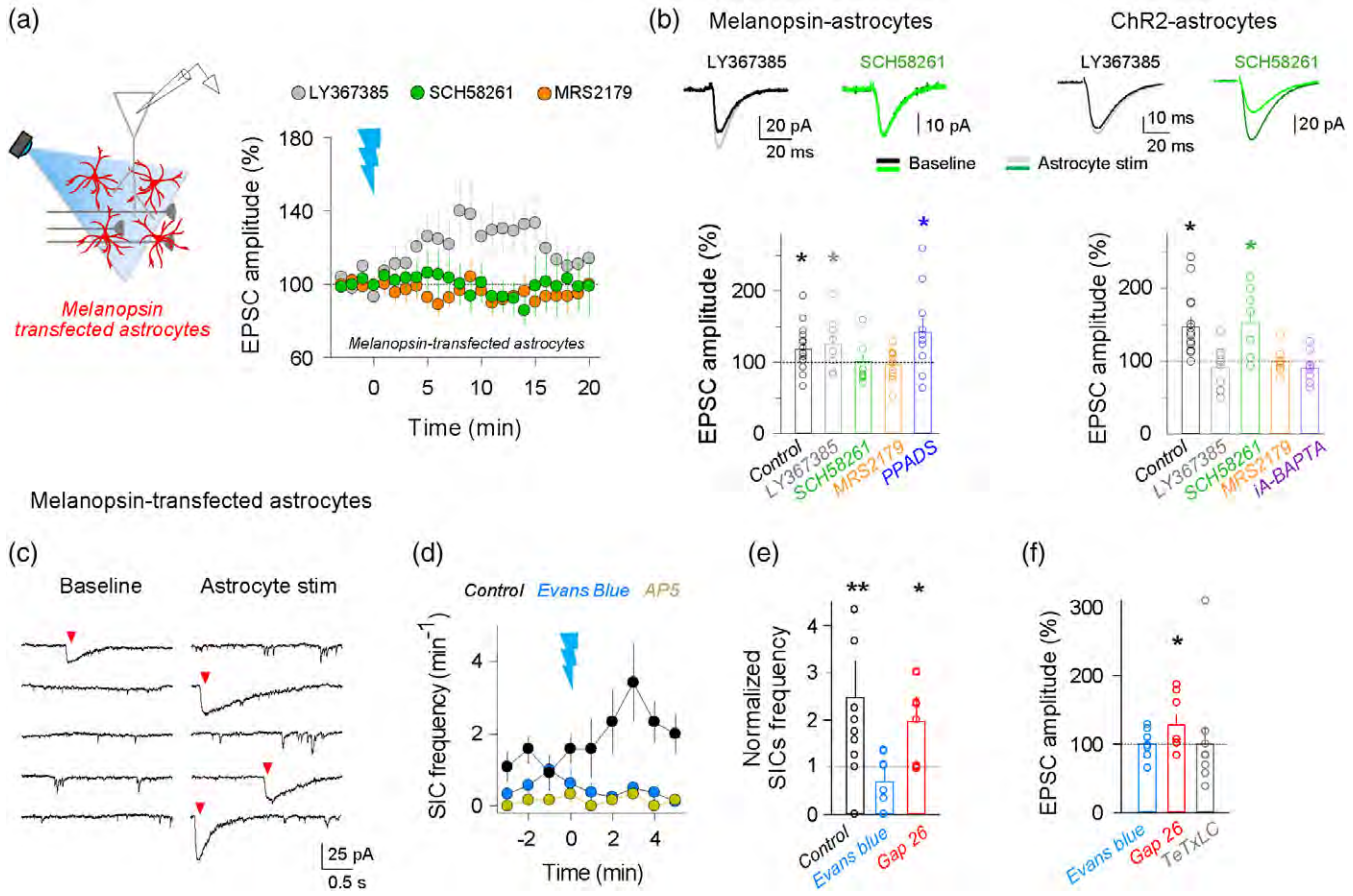

FIGURE 6 Melanopsin-driven purinergic and glutamatergic transmission triggers astrocyte-neuron signaling. (a) Schematic drawing of experimental design. Changes in relative EPSC amplitude over time before and after 20 s of melanopsin-astrocyte stimulation in presence of LY 367385 (100 μM), SCH 58261 (10 μM), and MRS 2179 (10 μM). Zero time indicates light pulse (blue beam). (b) *Top*: representative EPSC recordings before and after (10 min) astrocyte stimulation in presence of LY 367385 (in black/gray) and SCH 58261 (in green). *Bottom left*: average of relative changes of EPSC amplitude induced by melanopsin-astrocyte stimulation (20 s light) in the presence of LY 367385 (n = 8; p = 0.046), SCH 58261 (n = 10), MRS 2179 (n = 12), and PPADS (n = 10); *p < 0.05; paired t test. *Bottom right:* changes of EPSC amplitude evoked by ChR2-astrocyte stimulation (20 s light) in the presence of LY 367385 (n = 11), SCH 58261(n = 8; p = 0.013), MRS 2179 (n = 8), and after intracellular astrocyte loading with BAPTA (n = 8). *p < 0.05; paired t test. (c) Representative recordings showing the increase of SICs frequency (red triangles) after 20 s melanopsin-astrocyte activation. (d) Mean SIC frequency over time after melanopsin-stimulation in control conditions (n = 12), or after loading astrocytes with of Evans Blue (n = 8) or with perfusion of D-AP5 (50 μM, n = 6). (e) Relative changes of the SIC frequency in control (n = 12; p = 0.007), in presence of Evans Blue (5 μM, n = 8), and Gap 26 (100 μM, n = 9, p = 0.016; *p < 0.05; **p < 0.01; paired t test). (f) Average of relative changes of EPSC amplitude by melanopsin-stimulation after intracellular astrocyte loading with Evans Blue (n = 8), Gap 26 (n = 8; p = 0.010) and LcTeTx (1 μM, n = 8). *p < 0.05; paired t test. Data are shown as mean ± *SEM*

(b) *Top*: representative raster plot of microdomain activity in *Ip3r2*$^{-/-}$ mice (n = 500), color coded according to fluorescence change, and average microdomain population activity versus time after 20 s of light stimulation (bottom, n = 589). (c) *Top*: histogram of ROIs event frequency versus time (20 s, n = 589). *Bottom*: percentage of ROIs showing an event during the first 20 s after light stimulation (1 s, n = 75; 5 s, n = 28; 10 s, n = 103, 20 s, n = 86; 19 slices from 4 mice). (d) Analysis of microdomain Ca^{2+} fluctuation properties showing mean responses for event frequency, amplitude and width (1 s, n = 238 out of 531 (44.82%); 5 s, n = 105 out of 405 (25.93%); 10 s, n = 359 out of 759 (47.30%); 20 s, n = 589 out of 789 (74.65%); 19 slices; from four mice). p > 0.05; one-way ANOVA, post hoc comparison with Tukey–Kramer test. Somatic Ca^{2+} signals were monitored with cyto-GCaMP6f at 20 s light pulses (n = 39 astrocytes, 10 slices from three mice). p > 0.05; one-way ANOVA, post hoc comparison with Tukey–Kramer test. Note the absence of light effects on Ca^{2+} signals. (e) Analysis of resting microdomains Ca^{2+} fluctuation properties from Lck-GCaMP6f wild-type melanopsin-astrocytes (black; n = 3,816) and *Ip3r2*$^{-/-}$ melanopsin-astrocytes (white; n = 1,291). Analysis of resting soma Ca^{2+} fluctuation properties from cyto-GCaMP6f wild-type melanopsin-astrocytes (black; n = 44) and *Ip3r2*$^{-/-}$ melanopsin-astrocytes (white; n = 39). ** p = 0.001; *** p < 0.001, one-way ANOVA, post hoc comparison with Tukey–Kramer test. (f) Schematic drawing of an experimental design for synaptic recordings, and percentage of neurons from *Ip3r2*$^{-/-}$ mice showing synaptic changes after astrocyte light stimulation. (g) *Top*: representative EPSC recordings before and after 20 s of astrocyte optical activation in *Ip3r2*$^{-/-}$ mice. *Bottom*: average of relative EPSC amplitude over time after astrocyte stimulation. Zero time indicates light pulse (blue beam). (h) Relative changes of EPSC amplitude in *Ip3r2*$^{-/-}$ mice by light pulses at different time points (1 s, n = 12; 5 s, n = 11; 10 s, n = 11; 20 s, n = 15). Values recorded at 10 min after light activation of *Ip3r2*$^{-/-}$-astrocytes with 1 s (mean: 105.55%; *SD*: 22.04%; *SEM*: 6.36%; n = 12), 5 s (mean: 100.88%; *SD*: 27.22%; SEM: 8.21%; n = 11), 10 s (mean: 97.41%; *SD*: 23.27%; *SEM*: 7.02%; n = 11) and 20 s (mean: 91.57%; *SD*: 14.82%; *SEM*: 3.83%; n = 15). p > 0.05; paired t-test. (i) Comparative analysis of EPSC changes evoked after wild-type and *Ip3r2*$^{-/-}$-melanopsin-astrocyte light stimulation with 20 s light pulses (10 min after stim). Note that *Ip3r2*$^{-/-}$-melanopsin astrocytes did not evoke EPSC changes compared with control-melanopsin astrocytes (p = 0.003; one-way ANOVA, post hoc comparison with Tukey–Kramer test). ** p < 0.01. Data are shown as mean ± *SEM*

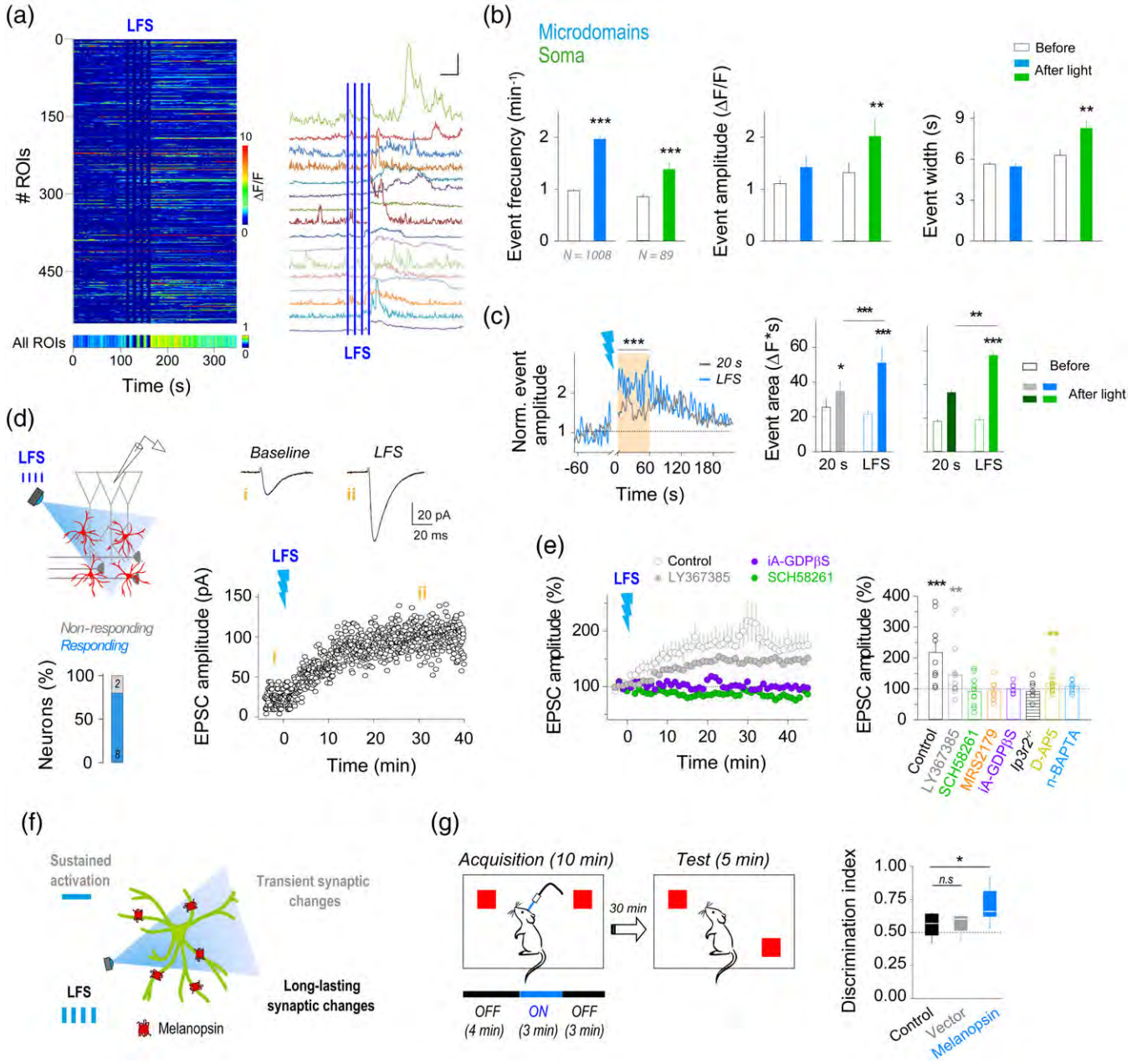

FIGURE 7 Low-frequency astrocyte activation drives hippocampal long-term synaptic plasticity and boosts memory performance. (a) *Left*: representative raster plot of microdomain activity, color coded according to fluorescence change (top, n = 500), and average microdomain population activity versus time (bottom, n = 1,008). *Right*: representative intensity of Ca^{2+} signals versus time evoked by melanopsin low-frequency stimulation (LFS; 5 s @ 0.06 Hz, 1 min; blue bars). Scale bar, 20 $\Delta F/F$, 35 s. (b) Blue bars, analysis of microdomain Ca^{2+} fluctuation properties showing mean responses for event amplitude, frequency (p < 0.001), and width (1,008 out of 1,182 events; 85.30%). p = 0.005 (**); p < 0.001 (***). Green bars, analysis of somatic Ca^{2+} fluctuation from cyto-GCaMPf6 viral expression showing mean responses for event amplitude (p = 0.003), frequency (p < 0.001), and width (p = 0.001; 18 slices from 3 mice). One-way ANOVA, post hoc comparison with Tukey–Kramer test. (c) *Left*: changes in the mean amplitude of Ca^{2+} event per active ROIs normalized to baseline over time, before and after 20 s light (n = 951) and LFS (n = 809; p < 0.001; one-way ANOVA, post hoc comparison with Dunns's test). *Right*: Ca^{2+} event area before and after 20 s light (p = 0.016) and LFS in astrocyte processes (gray and blue bars) and somas (green bars; p < 0.001; 20 s vs. LFS, p < 0.001). *p < 0.05; ***p < 0.001; two-way ANOVA, post hoc comparison with Dunn's test. (d) *Left*: schematic drawing of experimental design for synaptic recordings, and percentage of neurons showing synaptic changes after melanopsin LFS. *Right*: EPSC traces recorded before (i) and after (ii) astrocytic LFS, and EPSC amplitude over time from representative pyramidal cell. (e) *Left*: average of relative changes of EPSC amplitude over time after astrocyte LFS in control and in presence of LY 367385, astrocyte network-loading with GDPβS (iA-GDPβS), and SCH 58261. Zero time denotes light stimulation (blue beam). *Right*: relative mean values of EPSC amplitude after astrocyte LFS (mean value measured at 29–31 min) in control (n = 10, p < 0.001), and in the presence of LY 367385 (n = 10, p = 0.006), SCH 58261 (n = 11), MRS 2179 (n = 7), iA-GDPβS (n = 7), *Ip3r2*$^{-/-}$-melanopsin astrocytes (n = 7), D-AP5 (n = 13, p = 0.006), and intracellular BAPTA in neurons (n-BAPTA, n = 8). ** p < 0.01, *** p < 0.001, paired t test. Data are shown as mean ± *SEM*. (f) Scheme showing the ability of melanopsin-transfected astrocytes to decode duration and frequency of light protocols that originates modulatory synaptic responses with diverse temporal scales. (g) *Left*: Scheme of novel object location (NOL) test, indicating the timing of light protocol during the acquisition trial for both control (fiber-implanted nontransfected mice) and

of Ca^{2+} signals, but only events showing small Ca^{2+} amplitudes in resting conditions showed significant changes (Supporting Information Figure S9c). Using cyto-GCaMP6f, somatic Ca^{2+} events were also recorded and showed a robust increase after LFS stimulation (Figure 7b). Afterward, the efficacy to engage astrocyte Ca^{2+} signaling by 20 s light pulses and LFS was evaluated. The mean area of Ca^{2+} event amplitude was higher in both microdomains and soma after LFS (Figure 7c) indicating that melanopsin-activated astrocytes could discriminate light activity patterns driving different Ca^{2+} responses. In these conditions, recorded neurons displayed a robust EPSC potentiation after LFS that persisted after 30 min of recording (long-term potentiation, LTP) (80% of tested cells; 217.65 ± 37.51% from baseline; $n = 10$; $p < 0.001$; Figure 7d and e). The CV analysis indicated a presynaptic mechanism of action underlying LTP (Supporting Information Figure S9d). The astrocyte-mediated LTP was sensitive to the purinergic antagonist's SCH 58261 (91.39 ± 13.58% from baseline; $n = 11$; $p = 0.281$) and MRS 2179 (92.28 ± 12.54% from control; $n = 7$; $p = 0.396$; Figure 7e). The presence of mGluR1a antagonist LY 367385 failed to prevent synaptic potentiation (144.89 ± 15.36% from baseline; $n = 10$; $p = 0.006$; Figure 7e), although it was slightly reduced from control conditions ($p = 0.004$). The blockage of connexin-hemichannels and gap junctions with Gap26 (100 μM) did not prevent astrocyte-induced LTP (176.30 ± 22.79% from baseline; $n = 5$; $p < 0.001$; Supporting Information Figure S9e). However, LTP was abolished by intracellular loading of Evans blue (5 μM) into astrocyte network (91.08 ± 6.75% from baseline; $n = 7$; $p = 0.126$; Supporting Information Figure S9e). These data suggest a role for astrocytic ATP/Ado released by vesicular-dependent mechanisms in the melanopsin-induced synaptic plasticity. To establish the causal relationship between melanopsin-astrocyte Ca^{2+} signals and LTP, GDPβS was intracellularly loaded into the astrocytic network to downregulate G-protein signaling. After astrocyte GDPβS-loading, LFS failed to evoke LTP (100.12 ± 4.18% from baseline; $n = 6$; $p = 0.977$; Figure 7e). Likewise, stimulation of *Ip3r2*$^{-/-}$ melanopsin-transfected astrocytes (Supporting Information Figure S9b) failed to induce synaptic changes (91.76 ± 7.42% from baseline; $n = 7$; $p = 0.281$; Figure 7e); suggesting that astrocytic intracellular G-protein and IP3-dependent signaling were necessary and sufficient to induce LTP at hippocampal synapses.

NMDA receptors are broadly involved in LTP processes (Volianskis et al., 2015), and they have been related to particular forms of astrocyte-mediated synaptic plasticity (Adamsky et al., 2018; Henneberger et al., 2010; Min & Nevian, 2012). We found that in the presence of the NMDAR antagonist AP5 (50 μM), melanopsin-astrocyte stimulation still induced synaptic potentiation (118.68 ± 5.62% from baseline; $n = 13$; $p = 0.006$; Figure 7e and Supporting Information Figure S9d), but lesser extent than in control conditions ($p < 0.001$). Additionally, the contribution of postsynaptic activity was evaluated by intracellular loading of BAPTA into the recording neurons (nBAPTA; 20 mM). After nBAPTA-loading, astrocyte stimulation did not induce plasticity (108.60 ± 4.03% from baseline; $n = 8$; $p = 0.081$; Figure 7e and Supporting Information Figure S9d), suggesting that along with the presynaptic actions derived from optical astrocyte stimulation the postsynaptic neurons also contributed to the astrocyte-induced LTP. Interestingly, the analysis of former responses revealed a transient enhancement achieved during the first minutes after astrocytic LFS, similar to the short-term synaptic potentiation observed by acute melanopsin-astrocyte stimulation (Figure 2c). However, the activation of NMDARs and postsynaptic Ca^{2+} signaling were required for a sustained boost and LTP expression at hippocampal synapses (Volianskis et al., 2015; Supporting Information Figure S9d). Therefore, these data reveal the competence of astrocytes to directly trigger long-term plasticity in response to different patterns of activity (Figure 7f).

Because astrocyte activity has been related to cognitive performance (Florian, Vecsey, Halassa, Haydon, & Abel, 2011; Lee et al., 2014; Y. K. Li et al., 2012; Matos et al., 2015; Oliveira, Sardinha, Guerra-Gomes, Araque, & Sousa, 2015; Perea et al., 2014), we next investigated whether the synaptic changes induced by melanopsin-astrocytic activation might have an impact on animal behavior. Mice were injected bilaterally with AAV2/5-Gfap-melanopsin-mCherry to target hippocampal astrocytes. 3 weeks after surgery, memory performance was evaluated by testing Novel Object Location (NOL), in which mice were exposed to two objects for 10 min (acquisition trial), and 30 min later were re-introduced to the cage with one of the objects in a different location, during 5 min for exploration (Figure 7g). LFS light protocol was applied for 3 min during the acquisition trial. We have found that astrocyte activation resulted in a significant boost for the displaced object preference compared to control mice; that is, melanopsin-astrocyte activation enhanced discrimination index (0.57 ± 0.030 in control mice, fiber implanted, vs. 0.56 ± 0.041 in vector-transfected mice, $p = 0.868$; and 0.70 ± 0.037 in melanopsin-transfected mice, $p = 0.041$; $n = 5$, $n = 6$, and $n = 11$; respectively; Figure 7g). These data reveal the competence of astrocytes to improve memory performance (Adamsky et al., 2018), and the efficiency of melanopsin as an astrocytic optical tool for cognitive studies.

4 | DISCUSSION

Astrocytes have been shown to modulate neuronal activity by means of different mechanisms. Although its outcome is controversial (Bazargani & Attwell, 2016), the mechanisms related to intracellular Ca^{2+} signaling have received particular attention (Agulhon et al., 2013; Araque et al., 2014; Bindocci et al., 2017). Optogenetics appears as an ideal tool for accomplishing noninvasive, time-controlled, and cell-type specific perturbation in the brain. Thus, the specific manipulation of astrocytes by light could aid to uncover the astrocytic roles in brain function (Xie et al., 2015). Here, we have applied for the first time

melanopsin-transfected mice. Test trial was performed in the absence of light. *Right*: Whisker plot quantification of discrimination index of control (0.569 ± 0.030; $n = 5$, black), vector-transfected mice (0.560 ± 0.041; $n = 6$, gray; $p = 0.868$), and melanopsin-transfected mice (0.699 ± 0.037; $n = 11$, blue; $p = 0.041$, control vs. melanopsin) showing the enhancement of recognition index induced by astrocyte activation. *$p < 0.05$, one-way ANOVA, post hoc comparison with Tukey–Kramer test

melanopsin to astrocytes, a retinal G-protein-coupled photopigment, as an optical approach to precisely stimulate Ca^{2+} signals. A slow kinetics of melanopsin-driven light responses in retinal ganglion cells has been already described (Do et al., 2009; Mure et al., 2016), regulating cell excitability for several tens of seconds even after the light has been switched off, that allows an extended temporal integration frame in these neurons (Sexton et al., 2012). In this context, melanopsin features (high photosensitivity, regulation of intracellular Ca^{2+} dynamics, and slow kinetics) seem the ideal candidate to manipulate astrocyte physiology with optical tools. Our study reveals that light activation of melanopsin evoked reliable Ca^{2+} elevations at microdomain levels and membrane photocurrents related with Ca^{2+}-activated K^+ channels at a different range of light pulses. A correlation was found between Ca^{2+} event frequency and light pulse duration that might suggest the ability of astrocytes to adjust their excitability to different synaptic weights. Additionally, we found that Ca^{2+} events in astrocytic microdomains from *Ip3r2*$^{-/-}$ mice (Srinivasan et al., 2015) did not show further changes after light stimulation, confirming the ability of melanopsin to engage intracellular IP3 signaling in astrocytes. A new source of Ca^{2+} signaling in astrocytic microdomains has been recently described (Agarwal et al., 2017), where discrete Ca^{2+} events are mediated by transient openings of the mitochondrial transition pore, which can be also detected in the *Ip3r2*$^{-/-}$ mice (Agarwal et al., 2017). Whether this new mechanism can be recruited by melanopsin is still unresolved and would need further investigation. However, although light-evoked currents were still present in *Ip3r2*$^{-/-}$ astrocytes, which suggests that melanopsin might activate additional IP3R2-independent signals, no significant Ca^{2+} changes were found in both astrocytic microdomains and soma, and no synaptic changes were detected in neighboring neurons. Hence, these data support that the G-protein and IP3R2 signaling are the main intracellular pathways (Sherwood et al., 2017) involved in the melanopsin-driven astrocytic Ca^{2+} and synaptic responses. Considering that astrocytes express a wide repertory of G-protein-coupled receptors that are activated by synaptically released neurotransmitters, the use of melanopsin as optical tool represents a reliable approach to stimulate endogenous G-protein signaling pathways. Accordingly, synaptic plasticity was abolished by the presence of GDPβS and BAPTA into astrocyte network, confirming its dependence on intracellular G-protein and Ca^{2+} signaling.

Although light activation of OptoXRs, engineered chimeric receptors comprising the intracellular loops of adrenergic receptors fused to light-sensitive opsins (Airan, Thompson, Fenno, Bernstein, & Deisseroth, 2009), has been applied to astrocytes in culture and in situ (Figueiredo et al., 2014; Tang et al., 2014), and a recent paper comes out during the submission of this study showing their impact for hippocampal memory performance (Adamsky et al., 2018); the molecular pathways and subcellular features of the activation of light-sensitive G-protein have not been explored. Here, we provide a thorough characterization of the mechanisms of action of melanopsin on astrocyte Ca^{2+} physiology and synaptic transmission. While further studies will disclose the benefits and suitability of using OptoXRs or melanopsin, these data extend the existing optogenetic toolkit for astrocyte manipulation and neuron–glia studies both in situ and in vivo.

We reported that while glutamate-evoked NMDAR-dependent inward currents in CA1 neurons, ATP/Ado induced the synaptic enhancement by activation of $A2_ARs$ and $P2Y_1Rs$. The autocrine action of ATP has been previously shown in response to optoXRs (Figueiredo et al., 2014) and ChR2 stimulation (Shen et al., 2017) which might reconcile the responses driven by different receptors after melanopsin stimulation. As a result, optical astrocyte activation might stimulate ATP release that engaged surrounding astrocytes via $P2Y_1Rs$ stimulation, concluding with an excitatory synaptic enhancement driven by adenosine $A2_ARs$. Nevertheless, not all the melanopsin-induced Ca^{2+} signals were competent for gliotransmitter release and modulation of synaptic transmission, and EPSC potentiation was only observed after astrocyte activation above 5 s, suggesting the existence of a threshold for astrocyte neuromodulation.

Based on the present data light activation of melanopsin derived in glutamate and ATP/Ado release from astrocytes by Ca^{2+} and vesicular-dependent mechanisms (Henneberger et al., 2010; Jourdain et al., 2007; Min & Nevian, 2012; Perea & Araque, 2007; Schwarz et al., 2017); however, alternative and/or coexisting mechanisms could occur (Hamilton & Attwell, 2010). Potentially, additional effects induced by ATP signaling could take place simultaneously to the activation of P2Y1 and adenosine A2A receptors. That is, the purinergic signaling triggered by astrocytic P2Y1 would evoke glutamate release via TREK1 and Best1 channels activation, which are preferentially expressed at microdomains adjacent to glutamatergic synapses and engaged upon GPCR stimulation inducing NMDA-dependent to slow inward currents (Woo et al., 2012). Hence, a cooperative action between ATP and glutamatergic signaling would result in the recorded increase of SICs after melanopsin stimulation (Figure 6d and e). Additionally, ATP-derived excitatory currents via P2XRs could be considered as slow inward currents (SICs) (Lalo et al., 2014, 2016). D-serine release, along with glutamate, would be affected after blockage of vesicular-dependent pathways, which might derive in a reduction of the frequency of NMDA-dependent currents (Papouin, Henneberger, Rusakov, & Oliet, 2017; Rasooli-Nejad, Palygin, Lalo, & Pankratov, 2014).

Previous studies in hippocampal slices have shown that ATP released from astrocytes downregulates AMPA receptors at postsynaptic membranes via P2X receptor activation (Pougnet et al., 2014, 2016); however, the potentiation of EPSC amplitude observed in our study does not agree with the reported contribution of P2XR to hippocampal synaptic depression (Pougnet et al., 2014); and additionally, the synaptic enhancement was not abolished by PPADS, an antagonist of P2XR. Alternatively, ATP released by astrocytes can stimulate postsynaptic P2XRs activation and evoke purinergic synaptic currents that contribute to excitatory transmission (Lalo et al., 2016). Given the difficulties to monitor the purinergic component of fast EPSCs, low probability, and low amplitude events (Pankratov, Lalo, Verkhratsky, & North, 2007), we cannot totally exclude the contribution of P2XRs in the melanopsin-reported effects (Boue-Grabot & Pankratov, 2017); however, the magnitude of synaptic modulation observed under P2XRs blockage was similar to control conditions ($p = 0.190$; unpaired t test), which suggest that ATP released by astrocytes largely stimulates excitatory synaptic transmission via purinergic activation of P2Y1 and A2A receptors.

Optogenetic manipulation of astrocytes with ChR2 has been shown to modulate both intracellular Ca^{2+} signals and neuronal activity regulating neuronal firing rate (Gourine et al., 2010; Perea et al., 2014; Tan et al., 2017), as well as excitatory and inhibitory synaptic transmission (Perea et al., 2014; Sasaki et al., 2012) under robust light stimulation conditions; however, the consequences of shorter pulses have been less explored. In agreement with previous studies, we found that ChR2-evoked Ca^{2+} signals were triggered by long light pulses confirming the ability of ChR2 to stimulate astrocytes; but shorter stimuli showed a remarkably reduced control power on astrocyte Ca^{2+} signals. However, while different light stimuli of melanopsin-astrocytes triggered transient EPSC modulation (Figure 2), the impact of ChR2-astrocyte stimulation on synaptic transmission lasted longer (Figure 3), suggesting that, besides Ca^{2+} signaling, ChR2 activation might trigger additional mechanisms that restrict its ability to fine-tune synaptic transmission (Beppu et al., 2014). Therefore, this study shows that melanopsin and ChR2 display different capability to trigger astrocyte Ca^{2+} signals and to impact neuronal activity by releasing glutamate or ATP. Our data suggest that melanopsin and ChR2 modulate synaptic activity by different temporal scales, considering that compared with melanopsin, ChR2 significantly enhanced synaptic transmission, but displayed a limited capability to transiently perturb neuronal networks. Hence, to increase the available options for optical astrocytic stimulation, melanopsin offers wider conditions to induce either short or long-lasting synaptic changes. Furthermore, our data might indicate that the differences observed by using ChR2 and melanopsin, that is, magnitude and time course of synaptic changes, are evoked by different modes of gliotransmitter release, that is, diffuse or bulk gliotransmission triggered by ChR2 versus spot-like signaling between astrocytic processes and synapses triggered by melanopsin. Additionally, melanopsin-induced synaptic modulation shows similar temporal profile to the synaptic changes mediated by endocannabinoid and GABAergic endogenous activation of astrocytes (Martin et al., 2015; Perea et al., 2016), which suggests that melanopsin stimulation might recapitulate the astrocyte activation under physiological conditions.

The role of Ca^{2+} signals as the molecular code for astrocyte signaling is under debate (Araque et al., 2014; Bazargani & Attwell, 2016; Rusakov, 2015). While some studies based on the exogenous expression of Mas-related G-protein-coupled receptor A1 (MrgprA1) selectively in astrocytes (Agulhon, Fiacco, & McCarthy, 2010) have reported that MrgprA1 stimulation mobilized intracellular Ca^{2+} but failed to affect hippocampal synaptic transmission, recent studies have shown positive effects of specific MrgprA1 activation of astrocytes on glutamate transporter currents (Devaraju et al., 2013) and ATP-related animal behavior (Cao et al., 2013). Despite the controversy, our data suggest a key role of G-protein signaling and Ca^{2+}-dependent mechanisms for melanopsin-driven astrocyte-mediated synaptic modulation in synaptic transmission and animal behavior.

Yet more, considering that image acquisition used in this study is 1 Hz, it seems feasible that the frequency of Ca^{2+} events shown might be underestimated. Future studies using faster scanning or 3D recordings (Bindocci et al., 2017; Stobart et al., 2018) would monitor with better precision the melanopsin-induced Ca^{2+} dynamics in astrocytes.

Whether Ca^{2+} signaling can be regulated by local signals and neuronal demands is being comprehensively examined (Rusakov, 2015). In this study, using melanopsin as a trigger we first evaluated whether changes in astrocyte Ca^{2+} dynamics had an impact on the local neuronal network. We found that low-frequency stimulation (LFS; 0.06 Hz) of melanopsin evoked significant Ca^{2+} responses in astrocytic processes and soma, and unexpectedly, long-lasting changes in excitatory synaptic transmission (LTP). These results indicate that changes in duration (Figure 1f and g), and frequency (Figure 7) of light protocols used to stimulate melanopsin-astrocytes can modulate intracellular Ca^{2+} signals with different consequences on synaptic plasticity, from transient to long-lasting effects. Indeed, while a single 5 s pulse did induce transient EPSC potentiation, LFS evoked LTP. Hence, our data show that tuning their Ca^{2+} signals astrocytes can participate in different forms of synaptic plasticity, which could denote the contribution of astrocytes to particular brain states. Recently, it has been shown the role of astrocyte signaling in short- and long-lasting EPSCs potentiation triggered by different patterns of postsynaptic neuronal activity (Gomez-Gonzalo et al., 2015; Martin et al., 2015; Perea et al., 2016), as well as the astrocytic contribution to low-frequency states of cortical circuits, which may play a causal role in the control of cortical synchronizations (Poskanzer & Yuste, 2016). Our results showed that periods of low-frequency activity in astrocytes can engage long-term hippocampal synaptic plasticity. We next investigated whether those changes induced by melanopsin-astrocyte activation would impact animal performance in vivo. Remarkably, activation of astrocytes in vivo induced an enhancement of hippocampal-dependent memory tasks (NOL), which supports the role of astrocytes in cognitive processes (Adamsky et al., 2018), and their potential as cognitive enhancers.

Altogether, these results show melanopsin as a light-control trigger to manipulate astrocytic Ca^{2+} signaling, which can mimic the endogenous signaling pathways based on G-protein/IP3 activation triggered by neurotransmitter receptor stimulation. Additionally, present data show that fine-tuning of astrocyte signaling impacts synaptic transmission at different temporal scales, suggesting the ability of astrocytes to sense diverse patterns of neuronal activity. Such range of astrocyte activation might contribute to different forms synaptic plasticity and animal behavior. Future studies will reveal whether melanopsin may replicate endogenous astrocyte activity patterns, that will uncover the weight of astrocytes in particular brain functions, and alternatively, whether melanopsin can be applied to restore dysfunctional astrocyte-to-neuron signaling in animal models of human diseases. Overall, present data reveal melanopsin as a valuable optogenetic tool for neuron–glia studies.

ACKNOWLEDGMENTS

The authors thank Dr. J. Chen (UCSD, CA, USA) for providing IP3R2$^{-/-}$ mice; Dr. W. Buño, Dr. E. Martin and Dr. Araque for helpful comments; Dr. JA Esteban, C. Sánchez and M.A. Muñoz for helpful assistance with the two-photon technical assistance; Dr. M. Valero for MATLAB advice. This work was supported by PhD fellowship program (MINECO, BES-2014-067594) to S.M; and MINECO grants

(BFU2013-47265R; Intramural 201620I017; BFU2016-75107-P) to G.P.

AUTHOR CONTRIBUTION

S. M., M. M.-F. and G. P. performed two-photon calcium imaging experiments, S. M. and G. P. analyzed calcium data. S. M. and A. H.-V. performed electrophysiology experiments and analyzed data. S. M. performed the in vivo experiments. J. R.-F. performed immunohistochemistry analysis. A. Y. and E. B. designed and provided GFAP-melanopsin construct. M. N. supervised and contributed to the two-photon calcium imaging experiments. G. P. designed the study and wrote the paper. All authors discussed the results and contributed to interpretation of the data.

CONFLICT OF INTEREST

The authors declare no competing financial interests.

ORCID

Gertrudis Perea https://orcid.org/0000-0001-5924-9175

REFERENCES

Adamsky, A., Kol, A., Kreisel, T., Doron, A., Ozeri-Engelhard, N., Melcer, T., … Goshen, I. (2018). Astrocytic activation generates de novo neuronal potentiation and memory enhancement. *Cell*, *174*, 59–71. https://doi.org/10.1016/j.cell.2018.05.002

Agarwal, A., Wu, P. H., Hughes, E. G., Fukaya, M., Tischfield, M. A., Langseth, A. J., … Bergles, D. E. (2017). Transient opening of the mitochondrial permeability transition pore induces microdomain calcium transients in astrocyte processes. *Neuron*, *93*(3), 587–605. https://doi.org/10.1016/j.neuron.2016.12.034

Agulhon, C., Boyt, K. M., Xie, A. X., Friocourt, F., Roth, B. L., & McCarthy, K. D. (2013). Modulation of the autonomic nervous system and behaviour by acute glial cell Gq protein-coupled receptor activation in vivo. *The Journal of Physiology*, *591*(22), 5599–5609. https://doi.org/10.1113/jphysiol.2013.261289

Agulhon, C., Fiacco, T. A., & McCarthy, K. D. (2010). Hippocampal short- and long-term plasticity are not modulated by astrocyte Ca2+ signaling. *Science*, *327*(5970), 1250–1254. https://doi.org/10.1126/science.1184821

Airan, R. D., Thompson, K. R., Fenno, L. E., Bernstein, H., & Deisseroth, K. (2009). Temporally precise in vivo control of intracellular signalling. *Nature*, *458*(7241), 1025–1029. https://doi.org/10.1038/nature07926

Araque, A., Carmignoto, G., Haydon, P. G., Oliet, S. H., Robitaille, R., & Volterra, A. (2014). Gliotransmitters travel in time and space. *Neuron*, *81*(4), 728–739. https://doi.org/10.1016/j.neuron.2014.02.007

Bang, J., Kim, H. Y., & Lee, H. (2016). Optogenetic and chemogenetic approaches for studying astrocytes and gliotransmitters. *Experimental Neurobiology*, *25*(5), 205–221. https://doi.org/10.5607/en.2016.25.5.205

Bazargani, N., & Attwell, D. (2016). Astrocyte calcium signaling: The third wave. *Nature Neuroscience*, *19*(2), 182–189. https://doi.org/10.1038/nn.4201

Bennett, M. V., Garre, J. M., Orellana, J. A., Bukauskas, F. F., Nedergaard, M., & Saez, J. C. (2012). Connexin and pannexin hemichannels in inflammatory responses of glia and neurons. *Brain Research*, *1487*, 3–15. https://doi.org/10.1016/j.brainres.2012.08.042

Beppu, K., Sasaki, T., Tanaka, K. F., Yamanaka, A., Fukazawa, Y., Shigemoto, R., & Matsui, K. (2014). Optogenetic countering of glial acidosis suppresses glial glutamate release and ischemic brain damage. *Neuron*, *81*(2), 314–320. https://doi.org/10.1016/j.neuron.2013.11.011

Bernstein, J. G., & Boyden, E. S. (2011). Optogenetic tools for analyzing the neural circuits of behavior. *Trends in Cognitive Sciences*, *15*(12), 592–600. https://doi.org/10.1016/j.tics.2011.10.003

Bindocci, E., Savtchouk, I., Liaudet, N., Becker, D., Carriero, G., & Volterra, A. (2017). Three-dimensional Ca(2+) imaging advances understanding of astrocyte biology. *Science*, *356*(6339), eaai8185. https://doi.org/10.1126/science.aai8185

Boue-Grabot, E., & Pankratov, Y. (2017). Modulation of central synapses by astrocyte-released ATP and postsynaptic P2X receptors. *Neural Plasticity*, *2017*, 9454275. https://doi.org/10.1155/2017/9454275

Cao, X., Li, L. P., Wang, Q., Wu, Q., Hu, H. H., Zhang, M., … Gao, T. M. (2013). Astrocyte-derived ATP modulates depressive-like behaviors. *Nature Medicine*, *19*(6), 773–777. https://doi.org/10.1038/nm.3162

Chen, N., Sugihara, H., Kim, J., Fu, Z., Barak, B., Sur, M., … Han, W. (2016). Direct modulation of GFAP-expressing glia in the arcuate nucleus bi-directionally regulates feeding. *eLife*, *5*, e18716. https://doi.org/10.7554/eLife.18716

Devaraju, P., Sun, M. Y., Myers, T. L., Lauderdale, K., & Fiacco, T. A. (2013). Astrocytic group I mGluR-dependent potentiation of astrocytic glutamate and potassium uptake. *Journal of Neurophysiology*, *109*(9), 2404–2414. https://doi.org/10.1152/jn.00517.2012

Di Castro, M. A., Chuquet, J., Liaudet, N., Bhaukaurally, K., Santello, M., Bouvier, D., … Volterra, A. (2011). Local Ca^{2+} detection and modulation of synaptic release by astrocytes. *Nature Neuroscience*, *14*(10), 1276–1284. https://doi.org/10.1038/nn.2929

Do, M. T., Kang, S. H., Xue, T., Zhong, H., Liao, H. W., Bergles, D. E., & Yau, K. W. (2009). Photon capture and signalling by melanopsin retinal ganglion cells. *Nature*, *457*(7227), 281–287. https://doi.org/10.1038/nature07682

Eriksen, J., Chang, R., McGregor, M., Silm, K., Suzuki, T., & Edwards, R. H. (2016). Protons regulate vesicular glutamate transporters through an allosteric mechanism. *Neuron*, *90*(4), 768–780. https://doi.org/10.1016/j.neuron.2016.03.026

Faber, D. S., & Korn, H. (1991). Applicability of the coefficient of variation method for analyzing synaptic plasticity. *Biophysical Journal*, *60*(5), 1288–1294. https://doi.org/10.1016/S0006-3495(91)82162-2

Fernandez de Sevilla, D., Cabezas, C., de Prada, A. N., Sanchez-Jimenez, A., & Buno, W. (2002). Selective muscarinic regulation of functional glutamatergic Schaffer collateral synapses in rat CA1 pyramidal neurons. *The Journal of Physiology*, *545*(Pt 1), 51–63.

Figueiredo, M., Lane, S., Stout, R. F., Jr., Liu, B., Parpura, V., Teschemacher, A. G., & Kasparov, S. (2014). Comparative analysis of optogenetic actuators in cultured astrocytes. *Cell Calcium*, *56*(3), 208–214. https://doi.org/10.1016/j.ceca.2014.07.007

Florian, C., Vecsey, C. G., Halassa, M. M., Haydon, P. G., & Abel, T. (2011). Astrocyte-derived adenosine and A1 receptor activity contribute to sleep loss-induced deficits in hippocampal synaptic plasticity and memory in mice. *The Journal of Neuroscience*, *31*(19), 6956–6962. https://doi.org/10.1523/JNEUROSCI.5761-10.2011

Geisler, J. C., Corbin, K. L., Li, Q., Feranchak, A. P., Nunemaker, C. S., & Li, C. (2013). Vesicular nucleotide transporter-mediated ATP release regulates insulin secretion. *Endocrinology*, *154*(2), 675–684. https://doi.org/10.1210/en.2012-1818

Goh, G. Y., Huang, H., Ullman, J., Borre, L., Hnasko, T. S., Trussell, L. O., & Edwards, R. H. (2011). Presynaptic regulation of quantal size: K+/H+ exchange stimulates vesicular glutamate transport. *Nature Neuroscience*, *14*(10), 1285–1292. https://doi.org/10.1038/nn.2898

Gomez-Gonzalo, M., Navarrete, M., Perea, G., Covelo, A., Martin-Fernandez, M., Shigemoto, R., … Araque, A. (2015). Endocannabinoids induce lateral long-term potentiation of transmitter release by stimulation of gliotransmission. *Cerebral Cortex*, *25*(10), 3699–3712. https://doi.org/10.1093/cercor/bhu231

Gordon, G. R., Baimoukhametova, D. V., Hewitt, S. A., Rajapaksha, W. R., Fisher, T. E., & Bains, J. S. (2005). Norepinephrine triggers release of glial ATP to increase postsynaptic efficacy. *Nature Neuroscience*, *8*(8), 1078–1086. https://doi.org/10.1038/nn1498

Gourine, A. V., Kasymov, V., Marina, N., Tang, F., Figueiredo, M. F., Lane, S., … Kasparov, S. (2010). Astrocytes control breathing through pH-dependent release of ATP. *Science*, *329*(5991), 571–575. https://doi.org/10.1126/science.1190721

Hamilton, N. B., & Attwell, D. (2010). Do astrocytes really exocytose neurotransmitters? *Nature Reviews. Neuroscience*, *11*(4), 227–238. https://doi.org/10.1038/nrn2803

Hatori, M., & Panda, S. (2010). The emerging roles of melanopsin in behavioral adaptation to light. *Trends in Molecular Medicine*, *16*(10), 435–446. https://doi.org/10.1016/j.molmed.2010.07.005

Hattar, S., Liao, H. W., Takao, M., Berson, D. M., & Yau, K. W. (2002). Melanopsin-containing retinal ganglion cells: Architecture, projections, and intrinsic photosensitivity. *Science*, *295*(5557), 1065–1070. https://doi.org/10.1126/science.1069609

Haustein, M. D., Kracun, S., Lu, X. H., Shih, T., Jackson-Weaver, O., Tong, X., … Khakh, B. S. (2014). Conditions and constraints for astrocyte calcium signaling in the hippocampal mossy fiber pathway. *Neuron*, *82*(2), 413–429. https://doi.org/10.1016/j.neuron.2014.02.041

Henneberger, C., Papouin, T., Oliet, S. H., & Rusakov, D. A. (2010). Long-term potentiation depends on release of D-serine from astrocytes. *Nature*, *463*(7278), 232–236. https://doi.org/10.1038/nature08673

Jourdain, P., Bergersen, L. H., Bhaukaurally, K., Bezzi, P., Santello, M., Domercq, M., … Volterra, A. (2007). Glutamate exocytosis from astrocytes controls synaptic strength. *Nature Neuroscience*, *10*(3), 331–339. https://doi.org/10.1038/nn1849

Karpuk, N., Burkovetskaya, M., Fritz, T., Angle, A., & Kielian, T. (2011). Neuroinflammation leads to region-dependent alterations in astrocyte gap junction communication and hemichannel activity. *The Journal of Neuroscience*, *31*(2), 414–425. https://doi.org/10.1523/JNEUROSCI.5247-10.2011

Lalo, U., Palygin, O., Rasooli-Nejad, S., Andrew, J., Haydon, P. G., & Pankratov, Y. (2014). Exocytosis of ATP from astrocytes modulates phasic and tonic inhibition in the neocortex. *PLoS Biology*, *12*(1), e1001747. https://doi.org/10.1371/journal.pbio.1001747

Lalo, U., Palygin, O., Verkhratsky, A., Grant, S. G., & Pankratov, Y. (2016). ATP from synaptic terminals and astrocytes regulates NMDA receptors and synaptic plasticity through PSD-95 multi-protein complex. *Scientific Reports*, *6*, 33609. https://doi.org/10.1038/srep33609

Lee, H. S., Ghetti, A., Pinto-Duarte, A., Wang, X., Dziewczapolski, G., Galimi, F., … Heinemann, S. F. (2014). Astrocytes contribute to gamma oscillations and recognition memory. *Proceedings of the National Academy of Sciences of the United States of America*, *111*(32), E3343–E3352. https://doi.org/10.1073/pnas.1410893111

Letellier, M., Park, Y. K., Chater, T. E., Chipman, P. H., Gautam, S. G., Oshima-Takago, T., & Goda, Y. (2016). Astrocytes regulate heterogeneity of presynaptic strengths in hippocampal networks. *Proceedings of the National Academy of Sciences of the United States of America*, *113*(19), E2685–E2694. https://doi.org/10.1073/pnas.1523717113

Li, X., Zima, A. V., Sheikh, F., Blatter, L. A., & Chen, J. (2005). Endothelin-1-induced arrhythmogenic Ca2+ signaling is abolished in atrial myocytes of inositol-1,4,5-trisphosphate(IP3)-receptor type 2-deficient mice. *Circulation Research*, *96*(12), 1274–1281. https://doi.org/10.1161/01.RES.0000172556.05576.4c

Li, Y. K., Wang, F., Wang, W., Luo, Y., Wu, P. F., Xiao, J. L., … Chen, J. G. (2012). Aquaporin-4 deficiency impairs synaptic plasticity and associative fear memory in the lateral amygdala: Involvement of downregulation of glutamate transporter-1 expression. *Neuropsychopharmacology*, *37*(8), 1867–1878. https://doi.org/10.1038/npp.2012.34

Lin, J. Y. (2011). A user's guide to channelrhodopsin variants: Features, limitations and future developments. *Experimental Physiology*, *96*(1), 19–25. https://doi.org/10.1113/expphysiol.2009.051961

Mariotti, L., Losi, G., Lia, A., Melone, M., Chiavegato, A., Gomez-Gonzalo, M., … Carmignoto, G. (2018). Interneuron-specific signaling evokes distinctive somatostatin-mediated responses in adult cortical astrocytes. *Nature Communications*, *9*(1), 82. https://doi.org/10.1038/s41467-017-02642-6

Martin, R., Bajo-Graneras, R., Moratalla, R., Perea, G., & Araque, A. (2015). Circuit-specific signaling in astrocyte-neuron networks in basal ganglia pathways. *Science*, *349*(6249), 730–734. https://doi.org/10.1126/science.aaa7945

Martin-Fernandez, M., Jamison, S., Robin, L. M., Zhao, Z., Martin, E. D., Aguilar, J., … Araque, A. (2017). Synapse-specific astrocyte gating of amygdala-related behavior. *Nature Neuroscience*, *20*, 1540–1548. https://doi.org/10.1038/nn.4649

Masamoto, K., Unekawa, M., Watanabe, T., Toriumi, H., Takuwa, H., Kawaguchi, H., … Suzuki, N. (2015). Unveiling astrocytic control of cerebral blood flow with optogenetics. *Scientific Reports*, *5*, 11455. https://doi.org/10.1038/srep11455

Matos, M., Shen, H. Y., Augusto, E., Wang, Y., Wei, C. J., Wang, Y. T., … Chen, J. F. (2015). Deletion of adenosine A2A receptors from astrocytes disrupts glutamate homeostasis leading to psychomotor and cognitive impairment: Relevance to schizophrenia. *Biological Psychiatry*, *78*(11), 763–774. https://doi.org/10.1016/j.biopsych.2015.02.026

McGregor, K. M., Becamel, C., Marin, P., & Andrade, R. (2016). Using melanopsin to study G protein signaling in cortical neurons. *Journal of Neurophysiology*, *116*(3), 1082–1092. https://doi.org/10.1152/jn.00406.2016

Min, R., & Nevian, T. (2012). Astrocyte signaling controls spike timing-dependent depression at neocortical synapses. *Nature Neuroscience*, *15*(5), 746–753. https://doi.org/10.1038/nn.3075

Mure, L. S., Hatori, M., Zhu, Q., Demas, J., Kim, I. M., Nayak, S. K., & Panda, S. (2016). Melanopsin-encoded response properties of intrinsically photosensitive retinal ganglion cells. *Neuron*, *90*(5), 1016–1027. https://doi.org/10.1016/j.neuron.2016.04.016

Navarrete, M., Perea, G., Fernandez de Sevilla, D., Gomez-Gonzalo, M., Nunez, A., Martin, E. D., & Araque, A. (2012). Astrocytes mediate in vivo cholinergic-induced synaptic plasticity. *PLoS Biology*, *10*(2), e1001259. https://doi.org/10.1371/journal.pbio.1001259

Oliveira, J. F., Sardinha, V. M., Guerra-Gomes, S., Araque, A., & Sousa, N. (2015). Do stars govern our actions? Astrocyte involvement in rodent behavior. *Trends in Neurosciences*, *38*(9), 535–549. https://doi.org/10.1016/j.tins.2015.07.006

Oya, M., Kitaguchi, T., Yanagihara, Y., Numano, R., Kakeyama, M., Ikematsu, K., & Tsuboi, T. (2013). Vesicular nucleotide transporter is involved in ATP storage of secretory lysosomes in astrocytes. *Biochemical and Biophysical Research Communications*, *438*(1), 145–151. https://doi.org/10.1016/j.bbrc.2013.07.043

Panatier, A., Vallee, J., Haber, M., Murai, K. K., Lacaille, J. C., & Robitaille, R. (2011). Astrocytes are endogenous regulators of basal transmission at central synapses. *Cell*, *146*(5), 785–798. https://doi.org/10.1016/j.cell.2011.07.022

Panda, S., Nayak, S. K., Campo, B., Walker, J. R., Hogenesch, J. B., & Jegla, T. (2005). Illumination of the melanopsin signaling pathway. *Science*, *307*(5709), 600–604. https://doi.org/10.1126/science.1105121

Pankratov, Y., Lalo, U., Verkhratsky, A., & North, R. A. (2007). Quantal release of ATP in mouse cortex. *The Journal of General Physiology*, *129*(3), 257–265. https://doi.org/10.1085/jgp.200609693

Papouin, T., Henneberger, C., Rusakov, D. A., & Oliet, S. H. R. (2017). Astroglial versus neuronal D-serine: Fact checking. *Trends in Neurosciences*, *40*(9), 517–520. https://doi.org/10.1016/j.tins.2017.05.007

Peinado, G., Osorno, T., Gomez Mdel, P., & Nasi, E. (2015). Calcium activates the light-dependent conductance in melanopsin-expressing photoreceptors of amphioxus. *Proceedings of the National Academy of Sciences of the United States of America*, *112*(25), 7845–7850. https://doi.org/10.1073/pnas.1420265112

Pelluru, D., Konadhode, R. R., Bhat, N. R., & Shiromani, P. J. (2016). Optogenetic stimulation of astrocytes in the posterior hypothalamus increases sleep at night in C57BL/6J mice. *The European Journal of Neuroscience*, *43*(10), 1298–1306. https://doi.org/10.1111/ejn.13074

Perea, G., & Araque, A. (2005). Properties of synaptically evoked astrocyte calcium signal reveal synaptic information processing by astrocytes. *The Journal of Neuroscience*, *25*(9), 2192–2203. https://doi.org/10.1523/JNEUROSCI.3965-04.2005

Perea, G., & Araque, A. (2007). Astrocytes potentiate transmitter release at single hippocampal synapses. *Science*, *317*(5841), 1083–1086. https://doi.org/10.1126/science.1144640

Perea, G., Gomez, R., Mederos, S., Covelo, A., Ballesteros, J. J., Schlosser, L., … Araque, A. (2016). Activity-dependent switch of GABAergic inhibition into glutamatergic excitation in astrocyte-neuron networks. *eLife*, *5*, e23062. https://doi.org/10.7554/eLife.20362

Perea, G., Yang, A., Boyden, E. S., & Sur, M. (2014). Optogenetic astrocyte activation modulates response selectivity of visual cortex neurons in vivo. *Nature Communications*, *5*, 3262. https://doi.org/10.1038/ncomms4262

Poskanzer, K. E., & Yuste, R. (2016). Astrocytes regulate cortical state switching in vivo. *Proceedings of the National Academy of Sciences of the United States of America*, *113*(19), E2675–E2684. https://doi.org/10.1073/pnas.1520759113

Pougnet, J. T., Compans, B., Martinez, A., Choquet, D., Hosy, E., & Boue-Grabot, E. (2016). P2X-mediated AMPA receptor internalization and synaptic depression is controlled by two CaMKII phosphorylation sites on GluA1 in hippocampal neurons. *Scientific Reports*, *6*, 31836. https://doi.org/10.1038/srep31836

Pougnet, J. T., Toulme, E., Martinez, A., Choquet, D., Hosy, E., & Boue-Grabot, E. (2014). ATP P2X receptors downregulate AMPA receptor trafficking and postsynaptic efficacy in hippocampal neurons. *Neuron*, *83*(2), 417–430. https://doi.org/10.1016/j.neuron.2014.06.005

Rasooli-Nejad, S., Palygin, O., Lalo, U., & Pankratov, Y. (2014). Cannabinoid receptors contribute to astroglial Ca(2)(+)-signalling and control of synaptic plasticity in the neocortex. *Philosophical Transactions of the Royal Society of London. Series B, Biological Sciences*, *369*(1654), 20140077. https://doi.org/10.1098/rstb.2014.0077

Roux, L., Madar, A., Lacroix, M. M., Yi, C., Benchenane, K., & Giaume, C. (2015). Astroglial Connexin 43 Hemichannels modulate olfactory bulb slow oscillations. *The Journal of Neuroscience*, *35*(46), 15339–15352. https://doi.org/10.1523/JNEUROSCI.0861-15.2015

Rusakov, D. A. (2015). Disentangling calcium-driven astrocyte physiology. *Nature Reviews. Neuroscience*, *16*(4), 226–233. https://doi.org/10.1038/nrn3878

Sakamoto, S., Miyaji, T., Hiasa, M., Ichikawa, R., Uematsu, A., Iwatsuki, K., … Moriyama, Y. (2014). Impairment of vesicular ATP release affects glucose metabolism and increases insulin sensitivity. *Scientific Reports*, *4*, 6689. https://doi.org/10.1038/srep06689

Sanchez-Mendoza, E. H., Bellver-Landete, V., Arce, C., Doeppner, T. R., Hermann, D. M., & Oset-Gasque, M. J. (2017). Vesicular glutamate transporters play a role in neuronal differentiation of cultured SVZ-derived neural precursor cells. *PLoS One*, *12*(5), e0177069. https://doi.org/10.1371/journal.pone.0177069

Sasaki, T., Beppu, K., Tanaka, K. F., Fukazawa, Y., Shigemoto, R., & Matsui, K. (2012). Application of an optogenetic byway for perturbing neuronal activity via glial photostimulation. *Proceedings of the National Academy of Sciences of the United States of America*, *109*(50), 20720–20725. https://doi.org/10.1073/pnas.1213458109

Schwarz, Y., Zhao, N., Kirchhoff, F., & Bruns, D. (2017). Astrocytes control synaptic strength by two distinct v-SNARE-dependent release pathways. *Nature Neuroscience*, *20*, 1529–1539. https://doi.org/10.1038/nn.4647

Serrano, A., Haddjeri, N., Lacaille, J. C., & Robitaille, R. (2006). GABAergic network activation of glial cells underlies hippocampal heterosynaptic depression. *The Journal of Neuroscience*, *26*(20), 5370–5382. https://doi.org/10.1523/JNEUROSCI.5255-05.2006

Sexton, T., Buhr, E., & Van Gelder, R. N. (2012). Melanopsin and mechanisms of non-visual ocular photoreception. *The Journal of Biological Chemistry*, *287*(3), 1649–1656. https://doi.org/10.1074/jbc.R111.301226

Shen, W., Nikolic, L., Meunier, C., Pfrieger, F., & Audinat, E. (2017). An autocrine purinergic signaling controls astrocyte-induced neuronal excitation. *Scientific Reports*, *7*(1), 11280. https://doi.org/10.1038/s41598-017-11793-x

Sherwood, M. W., Arizono, M., Hisatsune, C., Bannai, H., Ebisui, E., Sherwood, J. L., … Mikoshiba, K. (2017). Astrocytic IP3 Rs: Contribution to Ca(2+) signalling and hippocampal LTP. *Glia*, *65*(3), 502–513. https://doi.org/10.1002/glia.23107

Shigetomi, E., Bowser, D. N., Sofroniew, M. V., & Khakh, B. S. (2008). Two forms of astrocyte calcium excitability have distinct effects on NMDA receptor-mediated slow inward currents in pyramidal neurons. *The Journal of Neuroscience*, *28*(26), 6659–6663. https://doi.org/10.1523/JNEUROSCI.1717-08.2008

Shigetomi, E., Bushong, E. A., Haustein, M. D., Tong, X., Jackson-Weaver, O., Kracun, S., … Khakh, B. S. (2013). Imaging calcium microdomains within entire astrocyte territories and endfeet with GCaMPs expressed using adeno-associated viruses. *The Journal of General Physiology*, *141*(5), 633–647. https://doi.org/10.1085/jgp.201210949

Srinivasan, R., Huang, B. S., Venugopal, S., Johnston, A. D., Chai, H., Zeng, H., … Khakh, B. S. (2015). Ca(2+) signaling in astrocytes from Ip3r2 (−/−) mice in brain slices and during startle responses in vivo. *Nature Neuroscience*, *18*(5), 708–717. https://doi.org/10.1038/nn.4001

Stobart, J. L., Ferrari, K. D., Barrett, M. J. P., Gluck, C., Stobart, M. J., Zuend, M., & Weber, B. (2018). Cortical circuit activity evokes rapid astrocyte calcium signals on a similar timescale to neurons. *Neuron*, *98*, 726–735.e4. https://doi.org/10.1016/j.neuron.2018.03.050

Tan, Z., Liu, Y., Xi, W., Lou, H. F., Zhu, L., Guo, Z., … Duan, S. (2017). Glia-derived ATP inversely regulates excitability of pyramidal and CCK-positive neurons. *Nature Communications*, *8*, 13772. https://doi.org/10.1038/ncomms13772

Tang, F., Lane, S., Korsak, A., Paton, J. F., Gourine, A. V., Kasparov, S., & Teschemacher, A. G. (2014). Lactate-mediated glia-neuronal signalling in the mammalian brain. *Nature Communications*, *5*, 3284. https://doi.org/10.1038/ncomms4284

Volianskis, A., France, G., Jensen, M. S., Bortolotto, Z. A., Jane, D. E., & Collingridge, G. L. (2015). Long-term potentiation and the role of N-methyl-D-aspartate receptors. *Brain Research*, *1621*, 5–16. https://doi.org/10.1016/j.brainres.2015.01.016

Woo, D. H., Han, K. S., Shim, J. W., Yoon, B. E., Kim, E., Bae, J. Y., … Lee, C. J. (2012). TREK-1 and Best1 channels mediate fast and slow glutamate release in astrocytes upon GPCR activation. *Cell*, *151*(1), 25–40. https://doi.org/10.1016/j.cell.2012.09.005

Xie, A. X., Petravicz, J., & McCarthy, K. D. (2015). Molecular approaches for manipulating astrocytic signaling in vivo. *Frontiers in Cellular Neuroscience*, *9*, 144. https://doi.org/10.3389/fncel.2015.00144

Yamashita, A., Hamada, A., Suhara, Y., Kawabe, R., Yanase, M., Kuzumaki, N., … Narita, M. (2014). Astrocytic activation in the anterior cingulate cortex is critical for sleep disorder under neuropathic pain. *Synapse*, *68*(6), 235–247. https://doi.org/10.1002/syn.21733

Yang, L., Qi, Y., & Yang, Y. (2015). Astrocytes control food intake by inhibiting AGRP neuron activity via adenosine A1 receptors. *Cell Reports*, *11*(5), 798–807. https://doi.org/10.1016/j.celrep.2015.04.002

SUPPORTING INFORMATION

Additional supporting information may be found online in the Supporting Information section at the end of the article.

How to cite this article: Mederos S, Hernández-Vivanco A, Ramírez-Franco J, et al. Melanopsin for precise optogenetic activation of astrocyte-neuron networks. *Glia*. 2018;1–20. https://doi.org/10.1002/glia.23580